PART I:
MECHNOBIOLOGICAL PROPERTIES OF THE EXTRACELLULAR MATRIX AND THE THERMODYNAMICS OF CANCER CELL INVASION

&

PART II:
STAND-OFF PULSE POWER PLASMA FUSION

A Dissertation
Presented to the Faculty of the Graduate School
of Cornell University
In Partial Fulfillment of the Requirements for the Degree of
Doctor of Philosophy

by
Joseph Patrick Miller
August, 2018

PART I

MECHNOBIOLOGICAL PROPERTIES OF THE EXTRACELLULAR MATRIX AND THE THERMODYNAMICS OF CANCER CELL INVASION

Joseph Patrick Miller
2018

Cells of all tissue types create and respond to mechanical signals in and from their surrounding extracellular matrix, respectively. However, only recently have the dynamics of this interplay been brought to the forefront of the scientific community's focus. The surprising finding of this effort, as it pertains to cancer, has been that cell-matrix interactions appear to be at least as critical to understanding the genesis and progression of the disease as are genetics or DNA mutation. The most immediately studied mechanical properties of the extracellular matrix include: the density of the matrix, alignment of the matrix fibers, stiffness of the fibers, and the tension on the fibers. The methods developed for controlling these variables have been numerous, however, few have succeeded in the deconvolution of the set. Here, novel experimentation, device construction, and theoretical treatments aimed to achieve this purpose are presented. The aggregate results of this dissertation argue that while these properties, which have historically been treated as separate mechanical cues in which a cancer cell must contend during invasion, are better interpreted through the single physical lens of energy expenditure. The conclusion is that cancer cells preferentially invade via the energy minimizing path and as such, can be at least partially inhibited by targeting the cells' external environment rather than exclusively its internal workings as has been the historical approach.

PART I

BIOGRAPHICAL SKETCH

Joseph P. Miller was born in City of Orange, Orange County CA August 3rd, 1982. He attended Mira Costa Community College from 2006 to 2008 before transferring to the University of California, Berkeley where he graduated with a double major in Physics and Economics in 2010. While completing his undergraduate work, Joseph worked in the Department of Nuclear Science at Lawrence Berkeley National Laboratories from 2009 to 2011. In 2011, he enrolled in the Biomedical Engineering doctoral program at Cornell University. He was awarded the Sloan Graduate Fellowship and the National Science Foundation Graduate Research Fellowship during this time. He obtained a Masters of Science in 2014 and continued on to pursue a PhD in Biomedical Engineering under the guidance of advisors Cynthia Reinhart-King, PhD; Amit Lal, PhD; and Susan Pannullo, MD.

PART I

To engineering for teaching me how to build a bridge.
To physics for teaching me how to burn it down.

And to my Mother and Wife, for teaching me when which is appropriate.

PART I

ACKNOWLEDGMENTS

First and foremost, I would like to acknowledge my mentor and thesis advisor, Cynthia Reinhart-King without whom I would certainly have drowned in unfocused curiosity. I want to acknowledge Amit Lal, who enabled me to explore the furthest reaches of my imagination and Susan Pannullo who brought me from bench to bedside and showed me the faces of the people this work impacts most directly.

I would like to acknowledge my funding sources: The National Science Foundation Graduate Research Fellowship, the Sloan Foundation Graduate Fellowship, the Kavli Institute of Nanotechnology, The Defense Advanced Research Project Agency (DARPA), the Advanced Research Project Energy – Energy (ARPA-E), the National Brain Tumor Society and the New York City Brain Tumor Project. I would like to thank Weill Cornell Medical College for hosting me for nearly two years while I shadowed Dr. Pannullo and the Laphroaig Distillery for exemplifying the definition of excellence.

Last but not least, I would like to acknowledge the many colleagues who contributed to this work both as scientists gathering data presented here and as authors and communicators of this data. Most notably, Francois Bordeluex, Matthew Zanotelli, Lauren Hapach, Jacob VanderWahl, Zachary Goldblatt, Shawn Carey, and Dylan Parker.

TABLE OF CONTENTS

iii. Biography
iv. Dedication
v. Acknowledgements

PART I
MECHNOBIOLOGICAL PROPERTIES OF THE EXTRACELLULAR MATRIX AND THE THERMODYNAMICS OF CANCER CELL INVASION

CHAPTER 1: Introduction - Cancer and the Extracellular Matrix
1.2 Alignment in the Extracellular Matrix
1.3 Tension in the Extracellular Matrix
1.4 Thermodynamics of Cancer Invasion
1.5 Dissertation Objectives

CHAPTER 2: Energy and the Extracellular Matrix
2.1 ATP:ADP Ratios as a Function of Glucose and Serum Levels
2.2 Matrix Density and Cancer Cell Energy Expenditure
2.3 Matrix Alignment Induces Cell Motility and Reduces Energy Expenditure
2.4 Contractility Inhibitors Reduce Intracellular ATP:ADP Ratios
2.5 Further Discussion and Conclusion

CHAPTER 3: Alignment, Tension and Stiffness in the Matrix
3.1 Separating Alignment from Tension
3.2 Alignment and Tension on Cell Polarization
3.3 Alignment and Tension on Tumor Spheroid Model Outgrowth
3.4 Alignment and Tension Effects on Cell Energy Expenditure
3.5 Theoretical Understanding
3.6 Further Discussion and Conclusion

CHAPTER 4: The Use of Clinical Radiation to Alter Tissue Mechanics
5.1 Mechanical Testing of Irradiated Cancerous Mammary Tissue
5.2 Mechanical Testing of Irradiated 3D Collagen Scaffolds
5.3 Infrared Radiation Spectroscopy of Irradiated Collagen Scaffolds
5.4 Cell Adhesion and Spreading on Irradiated Collagen Scaffolds

CHAPTER 5: Concluding Remarks & Future Directions
6.1 A Cell in Lineland
6.2 Activated Scaffolds
6.3 Final Thoughts

Appendix I – Protocols & Methods

PART I

Chapter 1

Introduction to Mechanobiology

An enormous amount of data has been generated regarding the inner workings and behavior of cells. Indeed, biology as a subject is one of the earliest studied forms of science. However, it has only been in the past few decades in which the field has expanded from the study of the cell and its inner workings to include the interaction between the cell and its environment, the extracellular matrix (ECM). In prior years, cell biologists either believed that a cell interacting in a collagen matrix, for example, was largely consistent between any given matrix or simply lacked the control of the matrix formation for proper experimentation. Fortunately, in more recent years, various mechanical parameters of the matrix such as density, alignment of the fibers that compose the matrix, tension on or the stiffness of those fibers have become the focus of biomedical engineers such that their importance to the cell-ECM dynamic and therefore to cell behavior in general has come into light (1–4). This new path of investigation, popularly referred to as "mechanobiology", opens the possibility for numerous other disciplines such as physics to provide leverage on critical biomedical challenges, including cancer.

The picture mechanobiology has painted is one of surprising impact. It now appears that the cell-ECM interaction is at least as important as the genetics of the cell in determining critical phenotypical behavior such as proliferation, apoptosis, differentiation and migration (5–8). In cancer, these behaviors correlate with invasive potential, disease severity and ultimately patient outcomes (9–11). As the mechanisms behind the cell-

ECM interaction have been illuminated, it is clear that the signaling path begins at the cell surface. Integrin-focal adhesion interactions kick off domino-like events through a cell's "senses"; moderated primarily though protein dynamics such as talin, vinculin, p130CAS, FAK, and MLP (12–14). This sensing process cascades into further downstream protein signaling, which then moderates gene expression in the nucleus (15). At this point, the cells eventual phenotype will manifest and clearly does so as a result of the initial sensing experience. Since a cell does not sense its environment in a vacuum, one can deduce that the ECM mechanical properties such as stiffness, alignment and tension, ultimately impact gene expression and cell behavior. This includes behavior that alters the ECM through the application of physical forces, creating an ever-present feedback loop (16).

While *in vivo*, the extracellular matrix is built of various proteins. Collagen is the most abundant in the human body and as such, has garnered a significant amount of focus in the field. Type I collagen, specifically, is the predominant structural component of the extracellular matrix in many tissues (17). For this reason, the body of work presented in this dissertation has built upon previous work using one-, two-, and three-dimensional collagen scaffolds as cell culture substrates to study the mechanisms governing cell invasion during cancer metastasis (3, 18, 19). Figure 1.1 illustrates a typical collagen scaffold. One can see that there is enormous variation in fiber length and width, pockets of high and low fiber density, areas of more or less fiber alignment and critically, as a function of all of those properties, variation in local stiffness and tension throughout the

matrix. Understanding the mechanical cues the cell receives from interacting with such variation is the focus and effort of the work presented here.

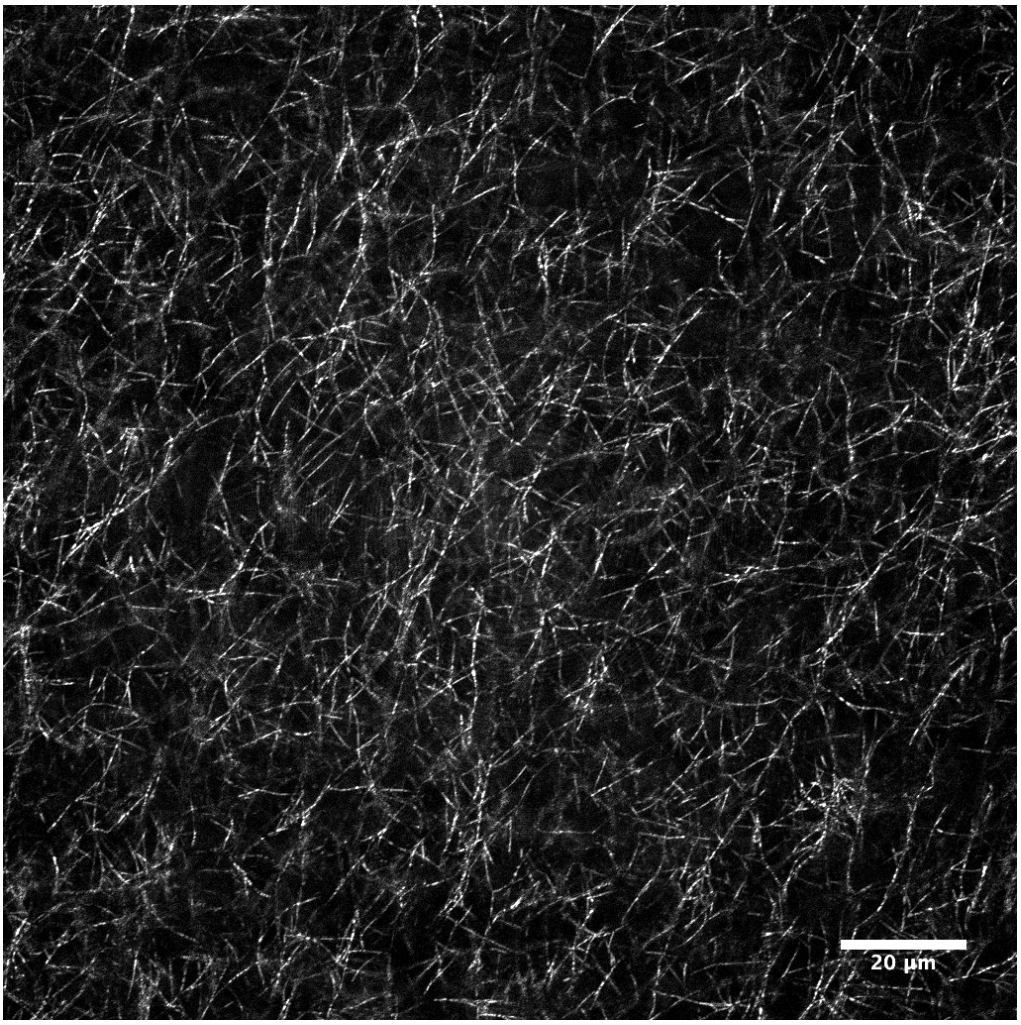

Figure 1.1: A typical collagen scaffold with variation in density, alignment and tension.

To begin making sense of how a cell might navigate such variation, it helps to understand the physics at play. The most pertinent equations for understanding fiber dynamics are those of stress and strain. Stress is defined as the force applied to an area. In the case of a fiber, ignoring bending modes, one may define stress as the force being pushed or pulled along the long axis of the fiber itself applied over the cross sectional area of the fiber

diameter. The strain of a stressed fiber is simply the amount the fiber stretches relative to its initial length. The ratio of stress and strain is called the Young's Modulus or elastic modulus of the fiber. This is an important measure, as it characterizes an intrinsic property of the material and is closely related to stiffness, which includes the additional complexity of structural details. It is the stiffness of the ECM in which the cell must contend, which forces us to understand the fiber-bundle dynamics that lead to the mechanical dynamics of the whole matrix.

In a matrix, groups of fibers form bundles. While these individual bundles may have approximately similar elastic moduli, the geometry of bundles adds additional complexity that has meaningful impact on the cell as it senses its environment. Most importantly, when a stress (Force/Area) is applied in the longitudinal direction of a bundle of fibers, instead of stretching the bundle, the dominant first-order behavior is to "unbundle" (20). This is similar to pulling a fork from a pile of spaghetti: at first, the force from the fork goes into unraveling the spaghetti, and only once the spaghetti is sufficiently unbundled, does it begin to "pull" on each strand. A cell experiences this very same interaction when applying stress to its surrounding matrix. At first, the fibers unbundle, and then additional stress induces what might appear to the cell as "strain hardening" – that is, the stiffness felt by the cell during the unbundling phase is less than the stiffness felt as the fibers elastically deform. This is a critical feature of the ECM-cell dynamic because if the cell is exerting energy for the purpose of translocation, much of that energy must first go into the unbundling and deformation of the surrounding matrix in the same way that one might imagine having to rope-climb a bungee cable. Until the bungee is sufficiently

taught, any stress applied to the cable will simply go into stretching the cable further. Only after strain hardening of the cable has set in, may the energy one expends go into actual motion of one's body. It for this very reason that, if presented with two cables: one made of rope (stiff) and one of bungee cord (soft), will a person chose the rope if he/she hopes to minimize the energy it takes for him/her to climb. With this intuition, one may turn their focus to the mechanical properties of a matrix that change the apparent stiffness of that matrix from the perspective of a cell.

1.2 Alignment in the Extracellular Matrix

Alignment has been shown to play a significant role in the migration and invasive signaling of cancer cells. For instance, in breast tissue, patients with more stromal collagen have significantly greater risk of developing breast cancer (21). The stromal collagen surrounding mammary tumor sites are often observed to be highly aligned perpendicular to the center of tumor's surface (22). This alignment facilitates cell invasion by creating tracks and increased stiffness, which we hypothesize frees up the energy a cell expends from deformation of the matrix to translocation of the cell body (23). As cells move through the alignment, force on the fiber is spread throughout the matrix via the network of fiber crosslinks, inducing further alignment, which creates a positive feedback loop to the sensing mechanisms of an invading cell.

It is important to note that in the absence of alignment, cells may pull on fibers closer to their transverse direction, where the fiber's dominant response is to bend. Bending modes play an important part in the stress distribution of the matrix. For example,

Ronceray et al. showed that these bending modes act as an amplifier of stress such that a local force from a cell or tumor can extend throughout the matrix orders of magnitude further than the diameter of the force causing unit (24). That is, a cell of roughly 10 microns in diameter can enact a force that is felt by other cells hundreds of microns away. Alignment of a matrix is effectively enabled by the unaligned fibers through this bending dynamic in two ways. First, bending the fibers obviously bends them into alignment with the direction of applied stress such that the result is a higher density of fibers in the aligned direction. Second, the force propagation throughout the matrix can recruit cells into applying stresses of their own in similar directions. The net effect of this group signaling can be profound and has been observed in the recruitment of cancer cell behavior.

1.3 Tension in the Extracellular Matrix

For all the mechanical properties present in a matrix, tension is the least studied in the field of mechanobiology. This is not because the field undervalues its importance, but because it is the most difficult to fabricate in a controlled manner suitable for experimentation. One of the primary issues is that sufficient tension on a collagen matrix will induce it to align (25). This convolutes tension with alignment and makes the study of their individual components challenging. Still, tension is known to have significant impact on cell behavior. Muscle contractions are tensile forces acting on the bones, lung tissue is known to stretch cyclically, and of course dermal tissue is constantly being stretched and affected by tensile forces. As it relates to the ECM, tensile forces have been shown to play a role in regulating MMP-2 mRNA expression (26, 27). Cycling this

tension force increased TNF-alpha production in human endothelial cells and TNF-beta production in rat cardiac fibroblast (28, 29). Related to cancer, tension has been shown to induce invasive behavior from tumor spheroid models and focus nearby cells to an invasive direction (30). The Liphardt lab at UC Berkeley found that by embedding two acini near one another in a 3D collagen matrix, tension fibers would form between the two acini, directing cell outgrowth. When these tension fibers were severed with two-photon ablation, the acini outgrowth patterns were radially uniform as if there were no other neighboring acini present (31). However, in all of these experiments, tension is confounded with alignment and the isolation of these factors is elusive. Further, the literature on tension in the ECM and how it affects cell behavior has treated it from the perspective of a causal player. In this dissertation, tension is not treated this way and is not considered any less of a player than alignment, density, or local stiffness. Since all of these are intermingled with the geometry of the matrix, it seems unlikely that it is just the tension or the alignment that is the *root cause* that leads the cell to behave differently. It is more likely that these confounding variables are actually mediators of a common cause. To understand the justification for that hypothesis, we need a more unifying principle.

1.4 Thermodynamics of Cancer Invasion

Thermodynamics is a strange term to hear in the field of cell biology. It is a term that invokes thoughts of combustion engines or burning stars. However, at the core, thermodynamics is simply the study of energy exchange between systems. In cancer biology, the invading cell and the ECM in which it invades are the systems of interest. In

the collagen matrix, each fiber is formed of a triple helix of smaller fibrils. Each of these fibrils is formed of repeating molecular blocks that interact with the other fibrils to form the stability of the larger fiber. All of this together can be thought of as something like a long series of linked bungie cables, springs in series form a single fiber. If the fibers are crosslinked, that crosslink is just a smaller spring putting two other springs in parallel. Equations describing the force response from pulling on one of these systems exists for each of these cases, but the base equation is the familiar Hooke's Law.

$$F = k\Delta x$$

In this simple equation, we can already begin to see all the mechanical properties previously discussed. Stiffness is defined by the constant *k*, tension force by the variable *F*. Alignment is revealed from the component analysis from this equation. That is, the product of *F* with the component of its vector (sine or cosine). When this equation is integrated along the direction of action, for example the distance a cell pulls a fiber, the energy consumed for that task is found.

$$U = \frac{1}{2}k\Delta x^2$$

As cancer cells invade through a network of fibers, this is the minimum energy each step consumes.

Approaching cancer mechanobiology from this perspective has only recently begun to reveal insights into the dynamics of invasion. Liu et al. revealed cells at the front of an invading population periodically rotate as a leader or a follower and most importantly, by doing so, minimize energy expenditure (32). Motivated by this work, the data presented in this dissertation argues it is exactly this goal invading cells are seeking to achieve.

Alignment, tension, and stiffness are simply variables of the more fundamental equation of energy and therefore the receptor and cytoskeletal sensing of mechanics in the ECM are not independent but rather products of a cell evolved to minimize energy expenditure.

1.5 Dissertation Objectives

The primary argument of this dissertation is that cancer cells display a preference to minimize the necessary energy expenditure of invasion. It is not the alignment, the stiffness or the tension that the cell is preferentially selecting for but the integration of the force in which each of these variables is a factor. Thus, therapies that target the ECM ought to be designed in a way that raises the energy cost of the cell to invade or behave abnormally. In the following chapters data is presented that establishes:

1. The intracellular ATP:ADP ratio is a reliable indicator of energy expenditure.
2. Cells preferentially invade in the direction of least energy expenditure.
3. Radiation is a clinical tool capable of increasing the energy cost associated with invasion.

Chapter 2

Energy and the Extracellular Matrix

Cancer cell invasion and migration during metastasis are hallmarks of cancer progression (9, 33). There is an interdependent relationship between cell adhesion and migration and the cellular microenvironment, where cells interact with their surrounding ECM, and in turn, the ECM mechanically changes in response to the cells' behavior (16, 34).

PART I

Mechanical cues from the ECM are sensed by the cell and converted to intracellular signals that direct cell protrusions, elongation, polarity, and migration efficacy (18, 35–37). Cells can sense and respond to an array of ECM cues including matrix alignment, stiffness, protein composition, and structural heterogeneities by altering their migration behavior (1–3, 38). Moreover, metastasis and metastatic cell migration are associated with an epithelial-to-mesenchymal transition, which is affected by both biochemical and mechanical cues within the cell and its local microenvironment (33, 39–43). To effectively migrate through the complex architecture of the stromal extracellular matrix (ECM) and ultimately to new locations throughout the body, cancer cells need to expend energy, generally via the dephosphorylation of ATP into ADP (44). However, the energy needs of cells during migration are not yet well understood.

Proper regulation of ATP/ADP levels is critical for cell health and essential cell functions (32, 33, 45–47). ATP is not kept in abundance or stored in cells like other biomolecules are, but rather its production is increased to match the demand of cellular activity (48–51). Previous literature has used molecular ATP sensors, such as PercevalHR, to observe and quantify energy levels inside cells during various cellular activities with a focus on metabolic processes including glycolysis and oxidative phosphorylation (52, 53). Not surprisingly, hindering, bypassing, or generating new metabolic pathways affect ATP levels (54–57). Changes in hypoxia also affect the levels of ATP and ADP (58–60). While our knowledge of ATP/ADP regulation is growing, currently there are no studies investigating ATP/ADP levels as a function of matrix architecture during migration.

PART I

We wanted to investigated how the microenvironment affects metastatic cell ATP generation during migration. To do so, we employ a fluorescent biomarker, PercevalHR (61), to determine how the ECM affects energy regulation in MDA-MB-231 cancer cells. PercevalHR binds to both conformations of ATP and ADP, and can be utilized to determine a concentration-independent ATP/ADP ratio as one metric of intracellular energy (45, 62). Interestingly, an increase in ECM density decreases cellular migration while simultaneously increasing the ATP/ADP ratio. In addition, aligned ECM matrices, known to facilitate cell migration (1), correlate with a decrease in the amount of energy produced by the cells. Pharmacological inhibition of motility by inhibiting contractility and actin polymerization resulted in a decrease in ATP/ADP. These results indicate that ECM architecture mediates energy production in cells, and the PercevalHR ATP/ADP probe is a promising tool for investigating cancer migration in live cell studies.

2.1 Cell Energy Expenditure in 2D and 3D Matrices

To validate that heightened metabolic activity correlated with increased ATP/ADP generation, MDA-MB-231 cells were seeded on plastic culture dishes and cultured in increased glucose and serum levels for 24hrs. Glucose increases ATP production via increases to both the substrate supply and Ca^{2+}–dependent activation of mitochondrial enzymes (50, 63). Here, cells were cultured in DMEM containing high excess glucose (25mM), which is approximately five times higher than physiological glucose levels. The PercevalHR biomarker was imaged to quantify the relative amounts of ATP and ADP inside migrating, live, single cells (Figure 2.1A). In high glucose but in the absence of serum, ATP/ADP ratios increased as a function of glucose concentration (Figure 2.1B).

Similarly, in standard (10%) serum levels, ATP/ADP levels increase with increased glucose levels. Increased glucose levels with serum present resulted in overall higher levels of ATP/ADP than without serum.

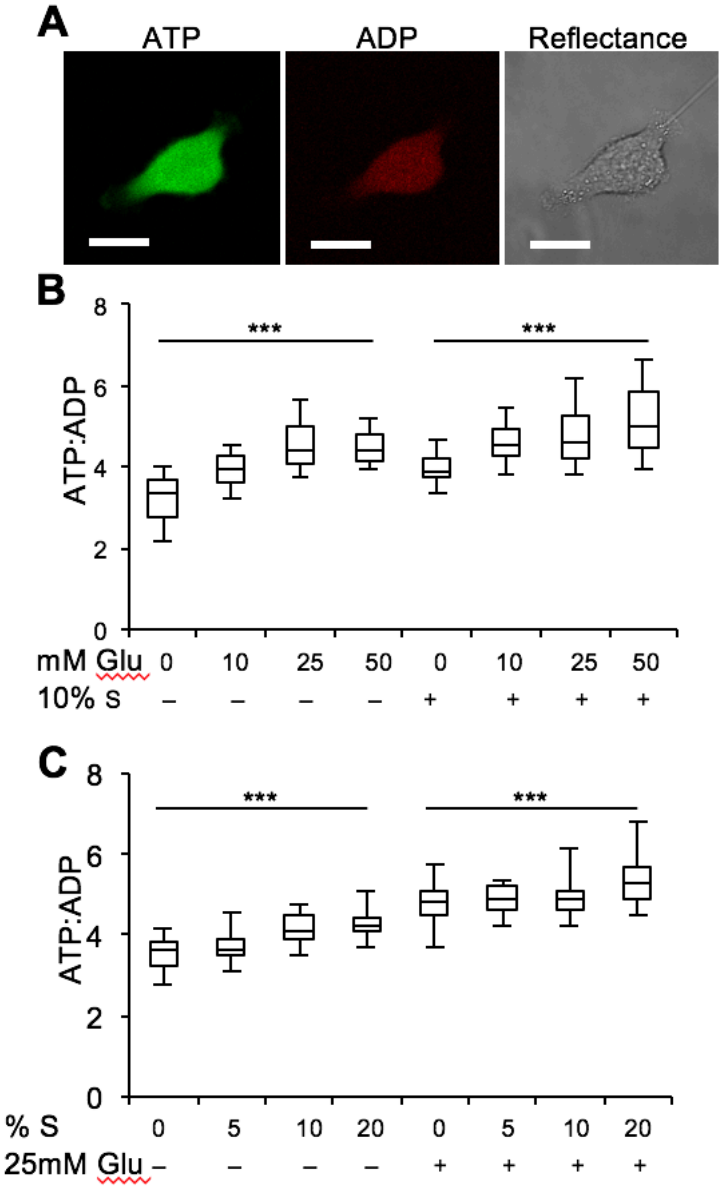

Figure 2.2: Cellular ATP response to glucose and serum in 2D.
Cellular ATP response to glucose and serum in 2D. **A)** Representative cell expressing the PercevalHR sensor in 2D culture showing the sensor bound to ATP (green), ADP (red), and the same cell in transmission (TPMT). **B)** Quantification of ATP:ADP ratio response to increasing glucose levels in the presence of 0% and 10% serum in 2D culture. **C)**

Quantification of ATP:ADP ratio response to increasing percent of serum in the presence of 0 mM and 25 mM glucose in 2D culture (n =45 cells from three independent experiments). Box and whisker plots show medians, $25^{th}/75^{th}$, and $5^{th}/95^{th}$ percentiles. Scale bars = 20μm. *** P<0.0001 for one-way ANOVA. (Figure provided by Zach Goldblatt.)

A similar result was seen when cells were cultured without glucose and increasing serum levels, where increased serum results in an increase in the ATP/ADP ratio. In high glucose, the ATP/ADP ratio significantly increased with increased serum levels. Increasing serum levels overall resulted in higher ATP/ADP ratios when glucose was present compared to when it was absent (Figure 2.1C). Together, these data indicate that the presence of high levels of glucose and serum allows cells to generate more ATP.

To investigate the effects of glucose and serum levels on the ATP/ADP ratio in cells seeded in 3D environments, MDA-MB-231 cells were cultured in varying glucose and serum levels for 24hrs in 3D collagen matrices and imaged to quantify the ATP/ADP ratio (Figure 2.2A). Similar to cells in 2D, in the absence of serum, glucose results in an increase in the ATP/ADP ratio (Figure 2.2B). In the absence of glucose, increased serum results in increased ATP/ADP ratio (Figure 2.2C). Together, these data indicate that stimulating cells that are embedded in 3D matrices with glucose or serum, which are known to increase metabolic activity, results in an increase in cellular ATP/ADP.

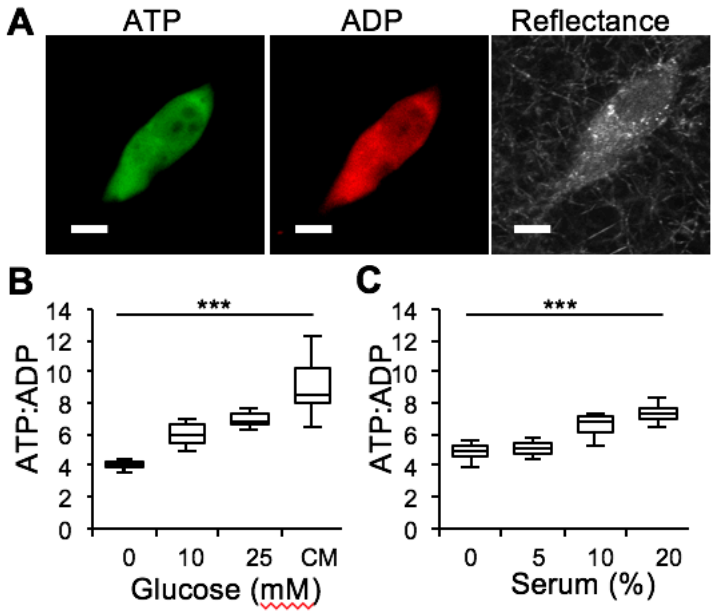

Figure 3.2: Cellular ATP response to glucose and serum in 3D matrices.
Cellular ATP response to glucose and serum in 3D collagen matrices. **A)** Representative cell expressing the PercevalHR sensor in 1.5 mg/ml 3D collagen gels. **B)** Quantification of ATP:ADP ratio response to increasing glucose levels in the presence of 0% serum in 3D collagen gels ($n \geq 20$ cells from three independent experiments). **C)** Quantification of ATP:ADP ratio in response to increasing serum levels in the presence of 0 mM glucose in 3D collagen gels ($n \geq 13$from three independent experiments). Box and whisker plots show medians, $25^{th}/75^{th}$, and $5^{th}/95^{th}$ percentiles. Scale bars = 30μm. *** $P<0.0001$ for one-way ANOVA. (Figure provided by Zach Goldblatt)

2.2 Matrix Density and Cancer Cell Energy Expenditure

To determine how matrix density affects the energetic state of cells, cells were seeded in 3D collagen matrices of different densities (1mg/mL, 3mg/mL and 5mg/mL) and both ATP/ADP ratio and cell speed were measured. Reflectance images were taken to visualize the fibrillar structure and density of the collagen without cells (Figure 2.3A) and with cells (Figure 2.3B). Cell speed decreased when matrix density increased for cells in both high and low glucose levels (Figure 2.3C). Most interestingly, cells exhibited significantly less ATP/ADP in 3D collagen matrices of lower density (Figure 3D). These

data suggest that cells require more energy for their migration and remodeling efforts in denser matrices where pore size is decreased.

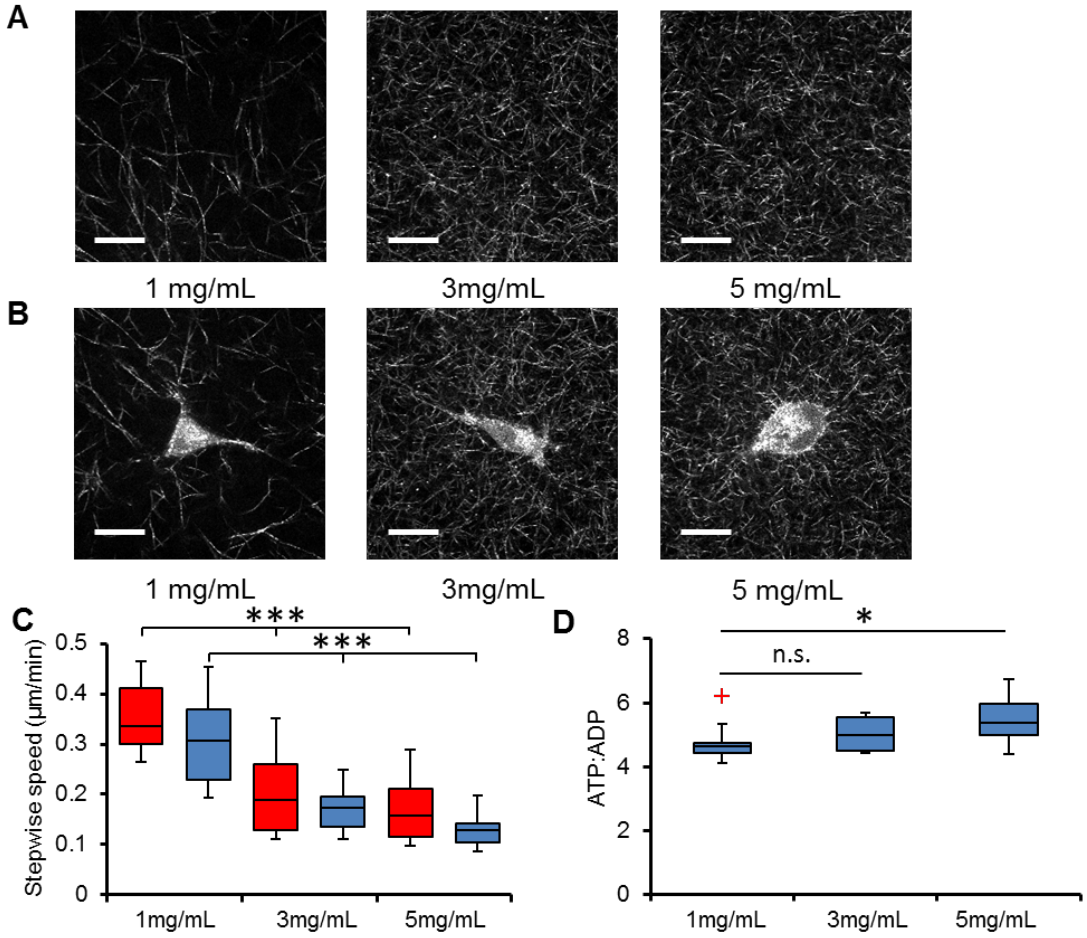

Figure 2.4: Effect of matrix density for ATP/ADP ratio and in migration in 3D. Confocal reflectance imaging of collagen gels with varying density without cells **(A)** and with cells **(B)**. **C)** Quantification of stepwise cell migration speed for increasing matrix density when cultured in DMEM with 10% serum and 25mM glucose (red) and DMEM with 10% serum and 0mM glucose (blue). n = 30 cells per treatment over three replicates. (Provided by Matt Zanotelli) **D)** Quantification of ATP/ADP ratio in cells for increasing matrix density when cultured in DMEM complete media. Red cross expresses an outlier. n = 10-20 cells per treatment over three replicates. Box and whisker plots show medians, $25^{th}/75^{th}$, and $5^{th}/95^{th}$ percentiles. Scale bar is 20µm. * P<0.05, *** P<0.0001

2.3 Matrix Alignment Induces Cell Motility and Reduces Energy Expenditure

Given that increased collagen density results in decreased matrix pore size and an increased ATP/ADP ratio, we sought to determine whether pre-organizing the matrix into a migration-permissive structure reduces the ATP demand and therefore results in a lower ATP/ADP ratio in cells. To test this hypothesis, we aligned collagen fibers (Figure 2.4A), which has been shown to facilitate migration both *in vitro* and *in vivo* (34, 36, 40, 64). Cell migration velocity increased in aligned matrices compared to randomly oriented matrices (Figure 2.4B). Accordingly, cells expressed significantly lower ATP/ADP ratios for aligned collagen matrices compared to those in random matrices (Figure 2.4C).

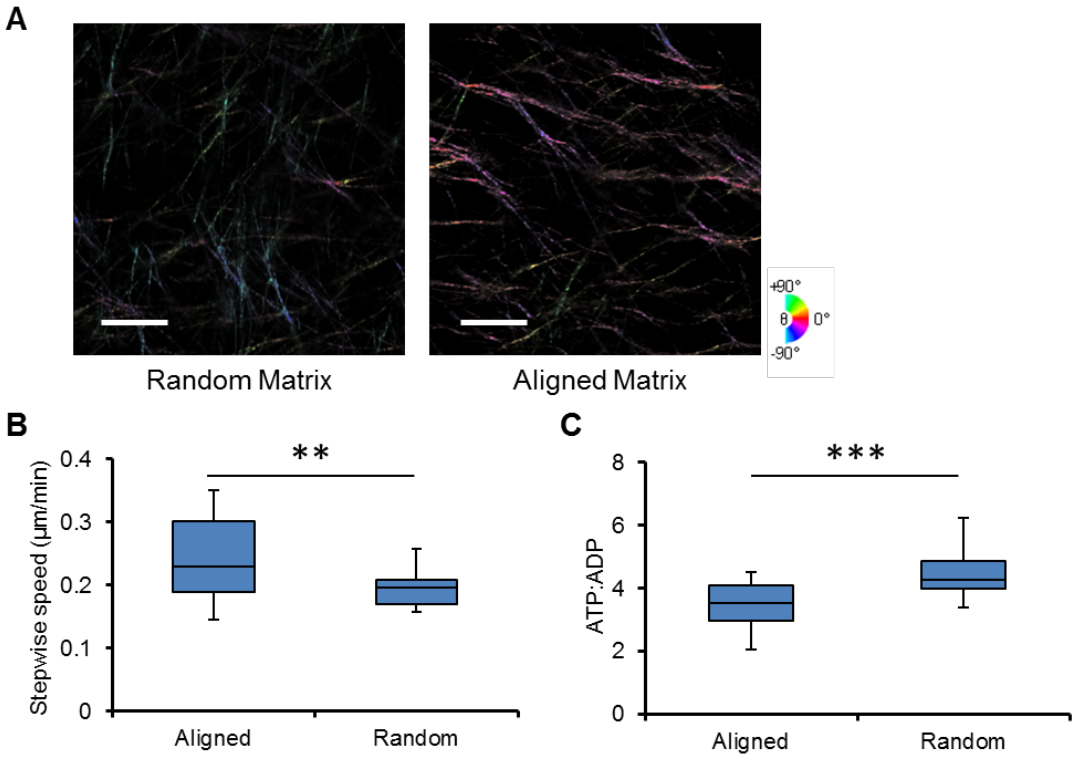

Figure 2.5: Reduction in ATP usage in cells by extracellular matrix alignment. **A)** Confocal reflectance imaging of collagen gel in random matrix (left) and aligned matrix (right). Collagen is pseudo-colored, corresponding to the fiber angle using OrientationJ in ImageJ. **B)** Quantification of stepwise cell migration speed in aligned and random extracellular matrix. n=30 cells per treatment for three replicates, ** $P<0.01$. **C)** Quantification of ATP/ADP ratio in cells in aligned and random extracellular matrix.

n=33 cells per treatment for three replicates, *** P<0.0001. Box and whisker plots show medians, 25th/75th, and 5th/95th percentiles. Scale bar is 20μm.

2.4 Contractility Inhibitors Reduce Intracellular ATP:ADP Ratios

Since cells require energy to migrate and cells typically produce ATP to fulfill their energetic needs (5,7), we hypothesized that if migration was inhibited, ATP/ADP ratio would decrease. To inhibit migration, we employed pharmacological inhibitors against ROCK, PI3-kinase, MLC kinase, and actin polymerization. ROCK is a key regulator of cytoskeletal organization, cell contractility, and migration (65). PI3-kinase is a major regulator of migration guidance in cells in relation to their extracellular environment (66). MLC kinase is a controlling factor in cell contractility, and LatA inhibitor prevents actin polymerization in the cytoskeleton (67, 68). Each of these inhibitors has been shown to reduce a cell's ability to spread and migrate in 3D. Our data indicate that cells treated with contractility/migration inhibitors exhibited a statistically significant decrease in ATP/ADP levels in both 2D (Figure 2.5A) and 3D culture (Figure 2.5B).

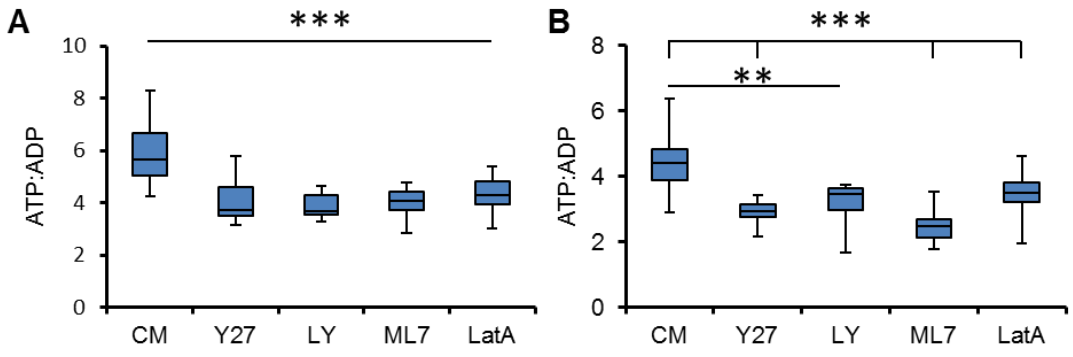

Figure 2.6: Reduction of ATP generation in cells by glucose inhibition.
Quantification of ATP/ADP ratio in cells in 2D **(A)** and 3D **(B)** while using various inhibitors in DMEM Complete Media. Box and whisker plots show medians, 25th/75th, and 5th/95th percentiles for n = 9-29 cells per treatment. **P<0.01, *** P<0.001 for each condition compared to the control.

2.5 Further Discussion and Conclusion

This work finds that in environments of higher-glucose levels, an environment known to increase cellular metabolism, cells generated increased levels of ATP. Energy is required for cell migration through the tumor stromal ECM *in vivo* and 3D collagen gels *in vitro*. The data indicated that more challenging ECM microenvironments (higher density collagen) result in increased energy levels in cells. Easing the migration effort by aligning the collagen fibers lowered the energy levels required for cells to move. Additionally, pharmacologically inhibiting motility and contractility functions lowered ATP/ADP ratios. Overall, these results describe how a cell's local environment affects its regulation of ATP and ADP levels, as well as its ability to migrate in 3D. All together then, these data suggest cells operate at demand driven levels of energy in order to migrate through various matrix conditions.

Many factors can change the amount of ATP/ADP inside of a cell, such as intracellular pH, stress, signaling activities, and metabolic and catabolic processes (61, 69–71). Here, pH variations were accounted for via the use of the pHRed sensor. The pHRed sensor allows the PercevalHR sensor to be normalized for pH variations due to various cell states, or biochemical micro-gradients in the ECM. The pair of these sensors proved to be sufficiently sensitive and effective at delineating between the various matrix conditions tested. Further, this effectiveness was independent from whether the cells were seeded in a 2D or 3D matrix, making them ideal for investigating the thermodynamic processes of cancer cell migration in 3D matrices.

Most interestingly, we observed an increase in energy expenditure for cells migrating through denser matrices. This result is in contrast to the inverse conclusion of Morris et al (72), where a decreased ATP level within the cell population in higher matrix densities was observed. One possible explanation is a selection bias between cells chosen for the studies reported here, which were live, single cells required to be protruding such that it was clear they were migrating, and the Morris study, which uses a boiling water method to dissolve the entirety of the cellular population. The latter likely includes cells that are dying on the gradient, dormant, possibly due to the high energy cost of migration through high-density collagen matrices, and maintaining correspondingly low levels of ATP.

This work helps explain how cancer cells utilize energy in order for efficient metastatic invasion, which is guided by varying microenvironmental conditions. There is significant research in how the tumor stromal ECM promotes tumor growth (73), metastasis from a primary tumor (40, 74), and tumor locoregional recurrence (75) Observing how cells interact with their ECM on a metabolic level, as well as how the ECM influences intracellular signaling as a result, can reveal new knowledge on cancer cell behavior and what cellular and molecular mechanisms may regulate this.

Future work includes understanding these differences more deeply as well as analyzing single cell rates of ATP change as they perform various tasks associated with the various cancer hallmarks. Specifically, one might look to the energy expenditure before, during, and immediately after vascular invasion or how energy regulation is optimized during group invasion.

In summary, the PercevalHR ATP/ADP sensor proves to be an effective and uniquely capable tool for studying the thermodynamics of live, single-cell cancer studies. Further, these data indicate the local microenvironment affects a cancer cells' ability to efficiently migrate through the ECM, as well as their regulation of metabolic processes such as energy generation and consumption. Denser ECMs impede the cell's ability to migrate and therefore increases the amount of energy the cell requires to move. Additionally, aligned ECM promotes cell migration by reducing the energy needed for cells to migrate. This study may have broad impacts on how cellular metabolic processes are affected by their environment, and specifically illuminate how the properties of the local ECM affect 3D cancer cell metastatic invasion and intracellular energy utilization. The PercevalHR biomarker has been shown to be a critical tool to this end and for future investigations of intracellular ATP/ADP levels as a means for understanding the metastatic energy requirements of cancer cells.

CHAPTER 3

Alignment, Tension and Stiffness in the Matrix

Cell invasion and migration is directed, in part, by mechanical cues within the microenvironment (43, 76–78). Recently, efforts have been made to identify and describe these mechanical cues to better understand the dynamic interactions between cells and the extracellular matrix (ECM) and their specific role in cancer cell invasion (16, 39, 40). Fiber alignment predicts protrusion orientation and speed of migration (79), as cells will preferentially migrate parallel to the direction of fiber alignment (1, 36, 80). These observations have all been indicated as being involved in early stages of the invasion process (1, 81). Cells actively use fibers to probe their environment (82) and long-range stress transmission between cells occurs across aligned collagen fibers (4, 83, 84).

While fiber alignment has been shown to direct migration, it has also been observed that tension in the matrix is detected by cells, and similarly, causes cells to polarize in the parallel direction (85, 86). Inhibition of actomyosin contractility as well as Rho-ROCK signaling reduces mammary acini spreading, and removal of mechanical interactions between acini completely blocks spreading (31). Furthermore, adjustments to matrix tension have previously been shown to alter cell shape (87), adhesion affinity (88), and actomyosin-mediated contraction, which are important processes during cancer cell migration (89).

Here, we hypothesize that cells preferentially invade along the energy-minimizing path. While alignment is thought to dictate cell motion, we hypothesize that because increased matrix tension reduces the energy required from the cell to translocate, tension dominates alignment in determining migration direction. To investigate this hypothesis, a PDMS cantilever was developed which both flow-aligns a fibrillar collagen matrix (90) and, when released, applies tension perpendicular to the aligned collagen. Using this device, we directly probed the relative roles of matrix alignment and matrix tension on cell migration.

3.1 Separating Alignment from Tension

To investigate the relative roles of matrix tension and matrix alignment in directing cell migration, the two variables must be experimentally decoupled. To apply tension perpendicular to the fibers without causing realignment, the resulting strain on any given fiber must be sufficiently small, such that the stress-strain state of the fiber exists just past the knee region and before the beginning of the linear elastic region; otherwise realignment of the fiber will occur (20). To this end, cantilever-shaped PDMS molds were built to flow-align collagen (Figure 3.1A). The alignment was verified by confocal reflectance and analyzed in ImageJ for fiber distribution utilizing Fourier analysis (91). The flow-induced alignment method produced a tight fiber orientation distribution nearly horizontal to the cantilever axis (Figure 3.1B). To induce tension, the cantilever was released and the collagen was reimaged 3 h later. Following cantilever release, the net orientation of fibers was unaffected (Figure 3.1C). As a means of validating the Fourier method of quantification, a random matrix was created within the device by depositing

collagen in multiple locations throughout the length of the device to prevent any flow from occurring. This produced a flatter, broader distribution with no significant alignment (Figure 3.1D). Within the flow-aligned matrices, the alignment persists throughout the entire depth that could be investigated with confocal reflectance microscopy, which is approximately 200 μm into the scaffold using our system (Figure 1E, F). Further, the dispersion of the orientation was consistent throughout the depth of analyzed collagen before and after applied tension (Figure 3.1G). Together, these data indicate that the cantilever is capable of flow-inducing alignment of collagen into a relatively tight distribution of orientated fibers that were insignificantly altered by its release and the subsequently applied tension (Figure 3.1H).

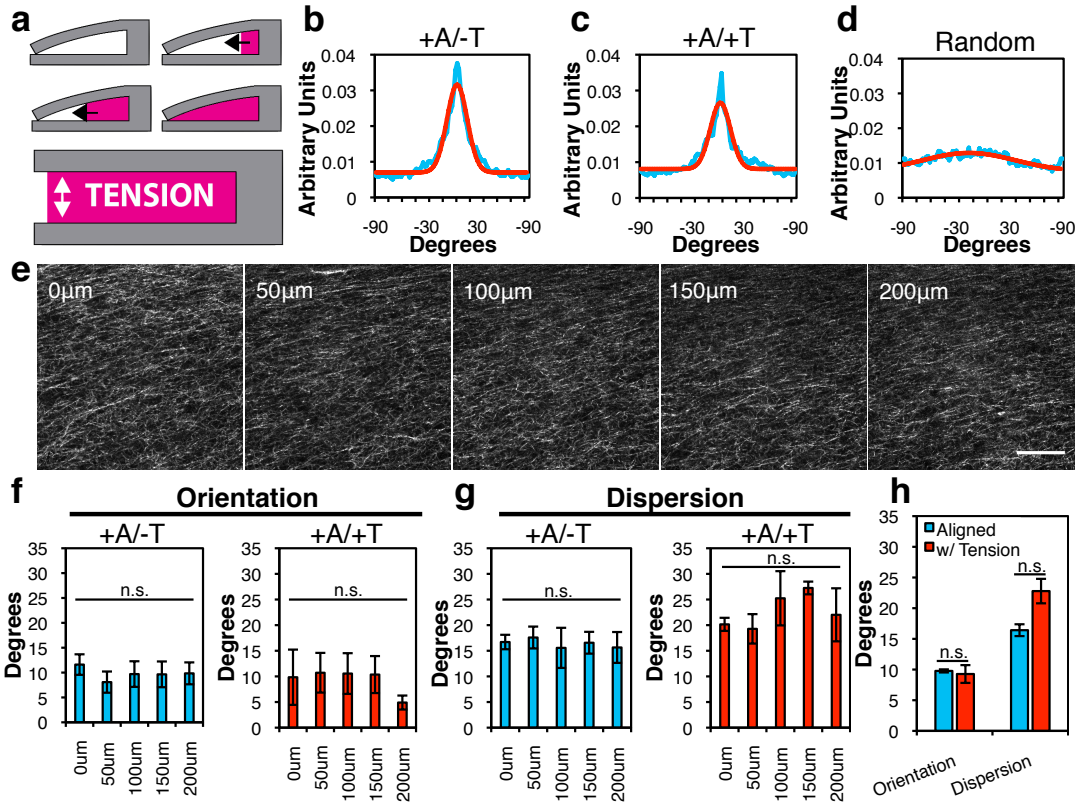

Figure 3.1: Tension from the PDMS Cantilever does not realign the matrix.

A) The flow-aligned process followed by the induction of tension by releasing the cantilever. **B, C, D)** Gaussian fit (red) of alignment distribution (blue) achieved with the flow-align process with and without tension compared to randomly aligned matrices (n = 3). **E)** Alignment persisted to the maximum depth capable of being imaged (200 μm) with reflectance microscopy. Scale bar = 25 μm. **F)** Orientation distributions by depth for aligned matrices with and without applied tension (n = 3). **G)** Corresponding dispersion distributions (n = 3). **H)** Average orientations and dispersions between aligned matrices with and without applied tension (n = 3). All bars report mean +/- S.D. Significance was calculated by ANOVA for figure **(F,G)**; student t-test for **(H)**.

3.2 Alignment and Tension on Cell Polarization

MDA-MB-231 breast cancer cells were embedded within collagen for 24 h prior to imaging. In the absence of tension, phalloidin staining revealed strong F-actin fiber orientation parallel to the aligned matrix (Figure 3.2A). Cell consistently polarized along the direction of fiber orientation (Figure 3.2B). Cell elongation angles, calculated to be the major axis of an algorithmically fitted ellipse to the cell body, closely coincided with the fiber orientation angle of approximately 10 +/- 15° (Figure 3.2C). Further, 24 h later, the same samples showed an increased number of cells within this range (Figure 3.2D).

When tension is applied by releasing the cantilever, actin stress fibers reoriented in the direction of tension (Figure 3.2E, F). Cell elongation angles also adjusted toward that of the tension vector (Figure 3.2G) with a similar long-term, reinforcing response where cell concentration narrowed around the tension direction (Figure 3.2H). Together, these data indicate that the application of tension to the matrix shifted the peak of the cell elongation angle distribution from 5–25° to 45–65°, amounting to approximately 40° change of the cell elongation angle towards the direction of tension.

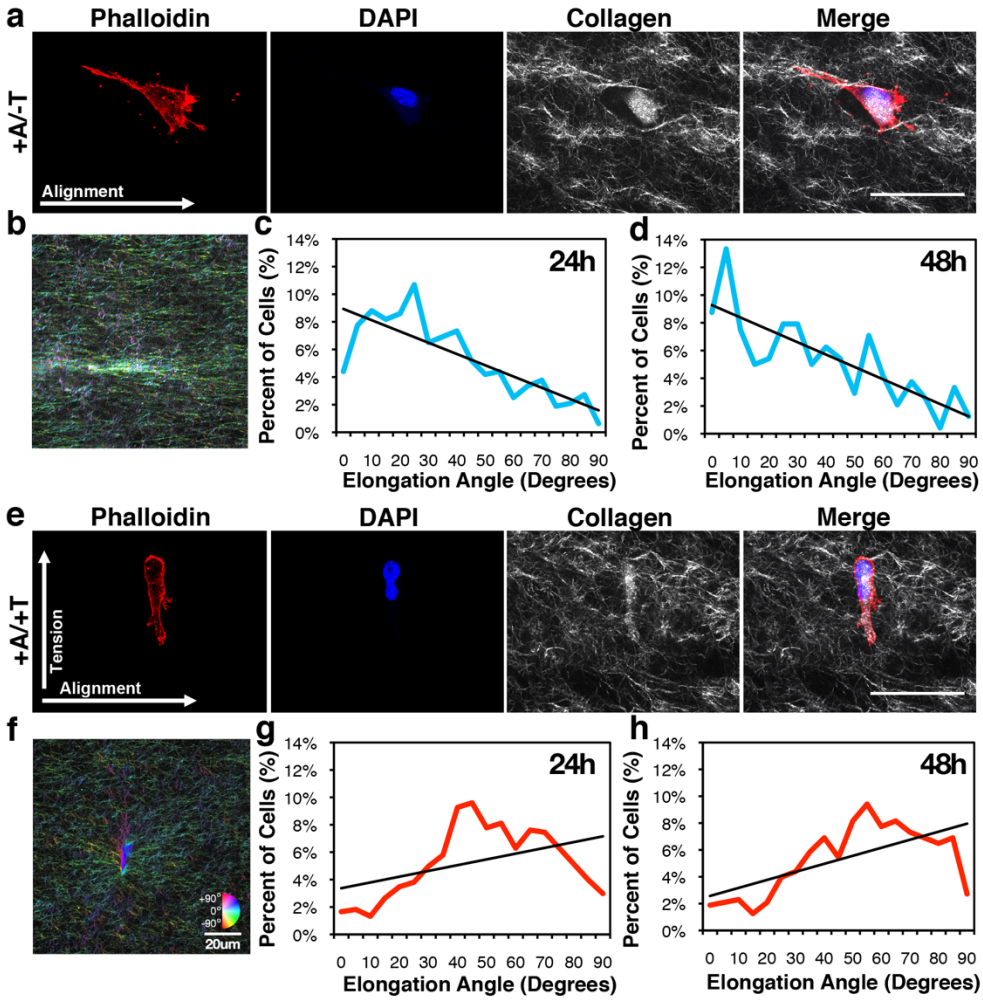

Figure 3.2: Tension causes the reorientation of cell elongation angles.
A) Phalloidin staining reveals actin fiber orientation in aligned matrices. Scale bar = 50 µm. **B)** Orientation-colorized image of cell in aligned matrix. C**)** Cell elongation distribution by angle relative to cantilever axis (0°) 24 h after seeding and (n=36) **(D)** 48 h after seeding with first order approximation, linear regression fit (n = 48). **E)** Confocal reflectance image of cell elongated along direction of tension. **F)** Orientation-colorized image of cell in aligned+tension matrix. **G)** Cell elongation distribution by angle 27 h after seeding (24 h + 3 h after applied tension) (n=36) and (**H)** 48 h after seeding (n = 48).

3.3 Alignment and Tension on Tumor Spheroid Model Outgrowth

Extending the study from single cells to a tumor spheroid model, measurements of outgrowth distance as a ratio in the two principle directions were examined. Aligned matrices yielded spheroids that preferentially outgrow in the aligned direction, random

matrices outgrow nearly equally in all directions, and spheroids in aligned matrices under perpendicular tension preferentially outgrow in the direction of tension (Figure 3.3A,B).

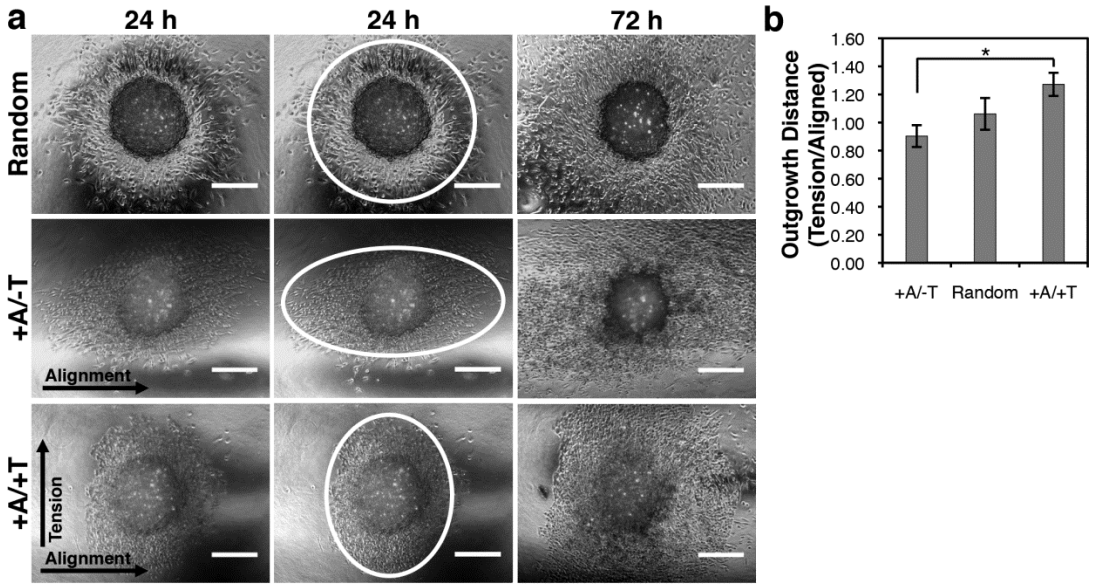

Figure 3.3: A) Top: Outgrowth in random matrix at 24 h, 24 h with fitted ellipse and 72 h. Middle: Outgrowth in aligned matrix without applied tension (+A/-T). Bottom: Spheroid outgrowth in aligned matrix in the presence of tension (+A/+T). Scale bar = 300 μm. **B)** Ratios of outgrowth in direction of tension to the outgrowth in direction of alignment at 24 h (student t-test: $p = 0.005$, $n = 3$).

Like single cells, spheroids actively realign their local ECM (92). Once this remodeling has occurred, the long-term outgrowth of the spheroid is biased by both cell-induced tension and cell-induced alignment. At 72 h, spheroids appear to maintain the outgrowth pattern established at 24 h. This suggests that external tension detected early by the cells composing the tumor model can have long term influence on the invasion pattern of the spheroid.

3.4 Alignment and Tension Effects on Cell Energy Expenditure

We hypothesize that the aligned direction of fibers is preferred by invading cells because it is thermodynamically efficient relative to a randomly oriented direction of fibers, and therefore a change from this direction in the presence of tension implies a new energetic minimum. To test this hypothesis, MDA-MB-231 cells were transfected with both the PercevalHR (61) ATP/ADP sensor, as a metric of energy production, as well as the pHRed (69) pH sensor, used to account for the pH sensitivity of PercevalHR (Figure 3.4A). Cells were imaged in aligned matrices with and without the applied tension (Figure 3.4B). Cells were also imaged in randomly oriented matrices as a control. The ATP/ADP ratio was minimized in cells invading in the direction of tension compared to the ATP/ADP ratio in cells in aligned or random matrices. These data indicate that cells require less energy to move in the direction of tension compared to alignment, which requires less energy than invasion in random matrices.

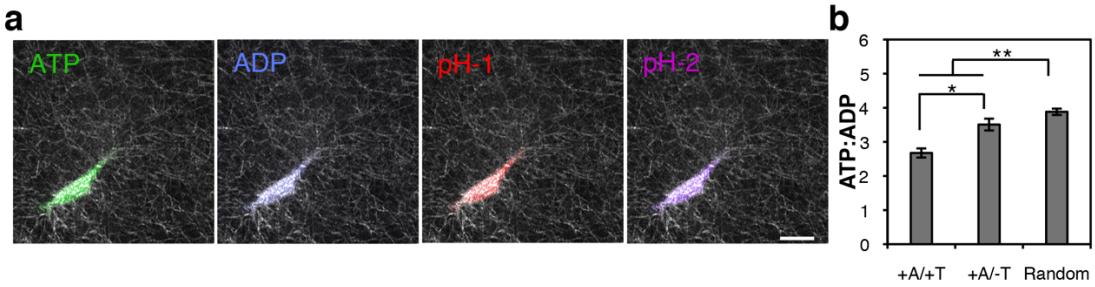

Figure 3.4: A) Fluorescent images of cells transfected with PercevalHR and pHRed sensor. **B)** ATP/ADP ratios accounting for pH in aligned matrices with applied tension, aligned matrices without applied tension, and random matrices (n = 93), scale bar = 20 μm.

3.5 Theoretical Understanding

To understand why tension reduces the energy required by invading cells, we approximated the force of the relaxed cantilever on the collagen fibers composing the

matrix. Uniaxial load testing was employed to deduce the spring constants (Figure 3.5A) of the PDMS molds. The spring constant (k_c) was found to be 61.57 +/- 14.36 N/m. The distance between the cantilever and the opposite wall (Δx) varies over the length of the cantilever; however, the displacement at the center of the cantilever is approximately 2.5 mm. The potential energy (U) stored in a compressed spring is given by:

$$U = \frac{1}{2} k \Delta x^2 \quad (1)$$

Thus, in the parallel-plate approximation, a spring with k_c of 60 N/m stores approximately 191 μJ of potential energy. Upon release of the cantilever, this energy must dissipate into the collagen matrix. Neglecting viscoelastic relaxation behaviors for a moment, the most basic model of a cantilever attached to a collagen matrix is a pre-compressed spring attached in series to a network of n smaller, initially relaxed springs (Figure 3.5B). Upon release, the cantilever relaxes to its resting equilibrium, and the potential energy distributes amongst the n springs via an increase in their individual Δx (Figure 3.5C). This suggests that an invading cell might migrate more efficiently through a matrix under tension where less of the cell's expended energy is converted into the deformation of the fibers and more can be directed toward the translocation of the cell body.

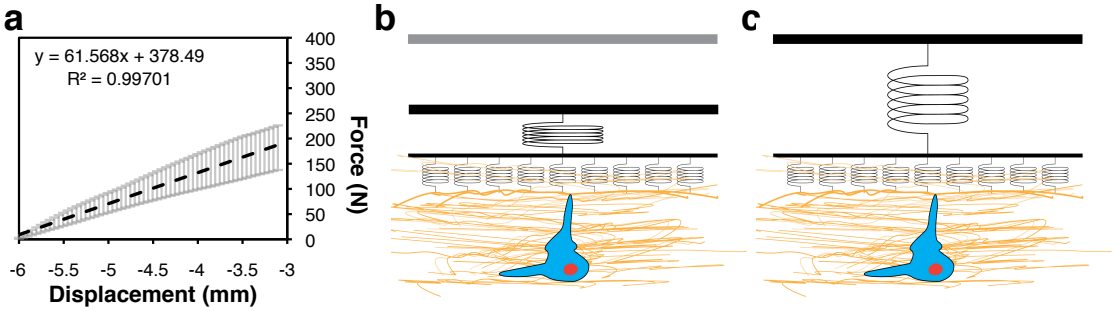

Figure 3.5: A) Force/displacement curves for PDMS cantilevers (n = 5, R^2 = 0.997). **B)** Model of cantilever coupling to a network of springs representing the collagen scaffold. **C)** After release of the cantilever, energy is distributed throughout the springs of the matrix.

Because any given fiber, or bundle of fibers, is being represented by a small spring, and this spring is ultimately in series with the cantilever, the effective spring constant of a fiber (k_f) and the cantilever (k_c) is given by,

$$k_{eff} = \left(\frac{1}{k_c} + \frac{1}{k_f}\right)^{-1} \quad (2)$$

This is the first-order spring constant the cell contends with when displacing a fiber by some amount in the direction of tension. Immediately, some qualitative observations can be made. Most notably, by adding the cantilever, each fiber has become *effectively* stiffer.

To attempt an estimate of the average tension in each fiber due to the cantilever (T_f), one performs the derivative of the potential energy, $= -\frac{\delta U}{\delta x}$, and divides by the number of fibers in the matrix (n):

$$T_f = \frac{k_{eff}\Delta x}{n} \quad (3)$$

To get an order of magnitude estimate for n, confocal reflectance images were taken with the pinhole set to image a 1.1 μm depth. The field of view was 200 μm x 200 μm. Using ImageJ, images were first made binary and skeletonized, then calculated to be on the order of 10^2 fibers. The volume of the collagen is given by ½ x 5 mm x 2.25 mm x 5 mm, as this is the volume of the space in the contracted cantilever arrangement approximated by a wedge. This total volume divided by the volume of the image that contained ~400 fibers yields an order of 10^8 fibers (n).

$$n = \left(V_C / V_{image}\right) * \left(Fibers\ in\ V_{image}\right) = \left(\frac{2.81*10^{-8}m^3}{4.40*10^{-14}m^3}\right) 400 = 2.56 * 10^8 \qquad (4)$$

A calculation of the cantilever force from Hooke's law distributed equally over 10^8 fibers in the matrix reveals the biasing tension to be approximately 600 pN of force per fiber in the antiparallel direction. This tension looks very similar in terms of the stored energy reported in the strain fields of an invading front of cells (93–95), but importantly, the cantilever has achieved this force without inducing matrix alignment. These data suggest that the cantilever applies a tension to the fibers that is physiologically relevant and within the range detectable and actionable by invading cancer cells.

3.6 Further Discussion and Conclusion

Matrix fiber tension and alignment have both been shown to direct cancer cell migration. However, tension gradients in the matrix are often coupled to a pre-aligned architecture, convoluting the impact of tension compared to alignment on cellular behavior. A PDMS

cantilever allows for the simultaneous creation of an aligned collagen matrix and the application of an anti-aligned tension force. Cell experiments revealed that tension dominates over net fiber alignment to provide directional migration cues to cancer cells. Use of an ATP/ADP molecular sensor revealed migration occurred in the direction of minimal energy expenditure. These data are the first to show that fiber tension dominates over alignment in directing cell motion, and that this is simply a result of energy minimization to the cell. The latter makes a significant contribution to unifying the seemingly competing findings regarding the role of tension and matrix alignment in directing cancer cell invasion.

Applied tension in the direction opposite to that of the net matrix alignment induced cancer cells to reorient and preferentially invade in the direction of tension. In addition, actin stress fibers reoriented toward the direction of tension relative to the aligned direction of the matrix. Similarly, in a spheroid tumor model, applied tension induced the spheroid to outgrow in the direction of tension. Once the spheroid begins outgrowth, the pattern of outgrowth was observed to be maintained over a 72 h period. Cell-induced collagen re-alignment has been shown in previous literature to act as a positive feedback for the invading population to recruit additional cells to invade in the same direction (9, 96, 97). Together, this implies an early response to external tension by tumor cells can result in long-term alterations to the outgrowth pattern of a metastatic site.

Previous studies have demonstrated that invading cells predictably and periodically exchange roles between leader and follower cells to minimize the thermodynamic cost of

invasion (32). Inspired by these results, the ATP/ADP sensor PercevalHR was employed to test whether the direction of applied tension is also the direction that demands the least energy expenditure. Indeed, the ATP/ADP ratio is lowest in cells migrating in a tensed matrix, suggesting that cells prefer to invade in a manner that minimizes energy expenditure. Further, modeling the system as a simplified network of springs revealed the magnitude of the force exerted on the fibers by the cantilever which induced directed migration is similar in terms of matrix-stored potential energy to what cells experience from an invading front (98).

Alignment and tension have been thoroughly investigated and found to have significant impact on cancer cell behavior (1, 80, 86). In addition, it is well appreciated that matrix stiffness plays a critical role in cell migration and cancer invasion (2, 22, 64). The effective stiffness a cell experiences is closely related to the tension and alignment of the probed fiber. Simulations accounting for the aspect ratio (diameter/length) of a long, flexible fiber reveal the effective stiffness along the axis (stretching mode) can be orders of magnitude greater than an identical probing force acting perpendicular to the axis (25, 99). Thus, a cell protrusion investigating a meshwork of fibers aligned in various angles senses vast heterogeneity of stiffness in its surroundings.

Historically, alignment, tension, and stiffness have been treated as independent factors influencing cell behavior. The more general conclusion of the data presented here is that these mechanical cues are united by Hooke's law where F is the tension in the fiber and k

is the stiffness of the fiber, which is modulated by the alignment of the fiber relative to the cell protrusion, θ. All together, the force a cell exerts on a fiber can be modeled by:

$$F_{cell} = k_{eff}\Delta x \cdot f(\theta) \qquad (5)$$

Thus, if a cell exerts the same force upon two fibers, the one that is stiffer, either because it is more highly cross-linked (increased k_{eff}) or because θ is aligned to the protrusion (fiber is in its stretching mode), will stretch (Δx) a shorter distance compared to the less cross-linked fiber or a fiber that was pulled at an angle that allowed for bending. Clearly, Δx must be less than some threshold in order for cell body translocation to occur; otherwise, the full force exerted by the cell would go into the deformation of the fiber, and only matrix compaction would result. Indeed, cells placed on ultra-soft matrices respond exactly in this way (100). Thus, as Δx gets smaller, more of the energy the cell exerts on the fiber can be converted into translocation of the cell body instead of the deformation of the fiber. Examining the energy a cell must exert by equation (1) clearly reveals that as Δx gets smaller, energy decreases by roughly the square root of Δx. A quick calculation based on the relative changes reported in the ATP/ADP ratios of cells in aligned matrices with and without tension (Fig. 4) reveals the change in Δx of the fibers to be only 9% less in fibers under tension compared to alignment alone. This is likely an overestimation once viscoelastic properties are taken into consideration. Together these data indicate that the mechanical cues of alignment, tension, and stiffness can be compared based on the energy the cell must exert when interacting with the fibers. For

the same energy expended, fibers in their aligned direction, fibers under tension, and stiffer fibers all stretch less, allowing the cell to translocate more efficiently.

It is important to note that collagen is not a purely linearly elastic material; it exhibits a time-dependent strain response (101). In a viscoelastic matrix, the elastic component will respond with a higher frequency as the stiffness of the matrix increases. When the matrix is biased with an externally applied tension, the time-dependent force response from a cell probing such a matrix may also play a role in the cells' ability to detect the energy-minimizing direction. It has already been shown that cells detect relaxation dynamics within the matrix and that it can have profound impact on cell differentiation (102).

Finally, it is possible that cells prioritize the investigation of the energy-minimizing path not only because it is efficient but because the tension sensed may also be a more information-dense measurement than the detection of local fiber alignment. That is, the detection of tension in a matrix delivers information about the matrix that is further away from the center of the cell, potentially millimeters away (25), whereas detection of what is locally aligned delivers only information about the matrix that is within micrometers of the cell and available to probe. Testing the limits of mechanical communication between cell bodies will be of particular value in understanding group invasive behavior and the coordination of invading cancer cells.

CHAPTER 4

The Use of Clinical Radiation to Alter Tissue Biomechanics

Recent studies conclude that cancer recurrence rates are highly correlated with the mechanical properties of the tumor microenvironment. Cells receive mechanical cues from their extracellular matrix (ECM) that direct migration, differentiation, apoptosis, and in some cases, the transition to a cancerous phenotype. Despite the prevalent use of radiation in the treatment of cancer and the significant research investigating how cells respond to radiation, very little is known regarding how radiation affects the ECM. The data presented here reveal that clinical doses of radiation alter the mechanical properties of collagen matrix by cleaving supporting peptide bonds in the individual collagen fibrils. Cleavage of these bonds results in a reduction of matrix stiffness to which cancer cells respond to with lower rates of adhesion, spreading, and invasion. Together, these data suggest that the application of radiation therapy could be expanded to include the targeting of tissue mechanical properties for the purposes of decreasing metastatic cell migration and potentially reducing recurrence rates.

Breast cancer is the leading cause of cancer related deaths in women 20-59 years of age (103). While the advent of many novel therapeutics and the advancement of early diagnostic imaging has significantly increased the 5-year life expectancy, the overall mortality rate has declined at a much slower rate; approximately 10% since 1930 (103, 104). This marginal decline in overall mortality suggests breast cancer recurrence is a continually looming threat and a poorly understood phenomenon. Indeed, long term

studies have reported that within 10 years nearly 40% of breast cancer patients will have some recurrence; 10-20% which manifest as locoregional recurrence, or in the immediate vicinity as the resected primary tumor (105, 106). It is thought that the population of cancerous cells left behind post-treatment is the primary cause of recurrence (11). Unfortunately, the treatment plans for recurrent patients are dismal at best and may be more limited depending upon the initial treatment plan and increased age of the patient. This is reflected in a decrease of the early-stage 10-year survival rate, from 93-100% to 56% (107). While significant progress has been made in the development of treatments of early stage breast cancer, the dangers of recurrence cannot be understated.

Interestingly, past clinical trials suggest that radiation beyond the standard of care can reduce recurrence rates and improve patient outcomes. Between 1989 and 1996, the European Organization for Research and Treatment of Cancer (EORTC) enrolled over 5000 stage I and II breast cancer patients who had undergone complete tumor resection to a clinical trial (108). In this trial, each patient was treated with a full breast exposure of 50Gy of radiation as is the standard of care (108, 109). However, half of these patients were delivered an additional dosage of radiation to the tumor bed. While the report offered no mechanism for the trial's success rate, patients that received the additional dosage experienced nearly half the recurrence rate compared to the control group over the full 8 years the patients were followed after treatment. Previous long-term, randomized trials reported similar findings between resection combined with post-surgical doses of radiation and resection alone (110–112). These trials, however, did not attempt to establish a mechanistic understanding of why the additional dose had the positive result

that it did beyond simply assuming it increased cancer cell death. To fully understand these clinical findings, knowledge of cell-radiation interactions must be augmented by an understanding of the effects of radiation on the ECM and how these changes affect cell-ECM interactions post-radiotherapy.

During tumor progression, increased ECM deposition and cross-linking occurs resulting in altered ECM composition, density, and stiffness (75, 80). This altered microenvironment has been shown to be a contributing factor to cancer development and progression. In breast cancer specifically, it has been demonstrated that increased ECM stiffness can induce a malignant phenotype in mammary epithelium (21). Unfortunately, to date, there is no locoregional targeting method aimed at altering ECM stiffness *in vivo* to mitigate these issues.

Here, we show that the utility of radiotherapy may extend beyond its typical clinical application of targeted cell death to include strategies that involve the altering of the mechanical properties of tissues. Motivated by work suggesting that radiation reduces the stiffness and strength of skin (113, 114), we investigated the effects of radiation on *ex vivo* mammary tumors from MMTV-PyMT transgenic mice. We found a dramatic reduction in stiffness post-radiation. Selecting for the tumors' primary scaffold component (collagen), we investigated the impact of radiation on the mechanical properties of an *in vitro* 3D collagen scaffold. Analyzing the microstructure of the scaffold, IR spectroscopy and confocal imaging was employed to analyze the chemical and architectural changes, respectively. Finally, experiments with non-irradiated MDA-

MB-231 mammalian breast cancer cells were carried out to isolate the cellular response to irradiated collagen from the response cells have to the radiation itself. Cell adhesion, cell spreading, and cell invasion were reduced in each compared to controls.

4.1 Mechanical Testing of Irradiated Cancerous Mammary Tissue

Inspired by the EORTC findings (115), we investigated the mechanical properties of post-irradiated mammary tumors in female MMTV-PyMT transgenic mice. Tumors were extracted from the mice and tested via mechanical compression. The results show a significant reduction in stiffness for irradiated tumors, as indicated by a flatter slope in the stress-strain curve generated during compression testing (Figure 4.1A). Further, there was a significant difference in tumor stiffness between groups irradiated with 63Gy (a typical dose delivered directly to the tumor) and 40Gy (a typical dose delivered to the tumor-stromal fringe), with the 40Gy treated tumors being slightly stiffer than the 63Gy treated tumors (Figure 4.1B). This result together with the fact the radiation source used produces monoenergetic photons, suggests the stiffness reducing effect is dose-dependent and a function of the time in which the sample is exposed to the source.

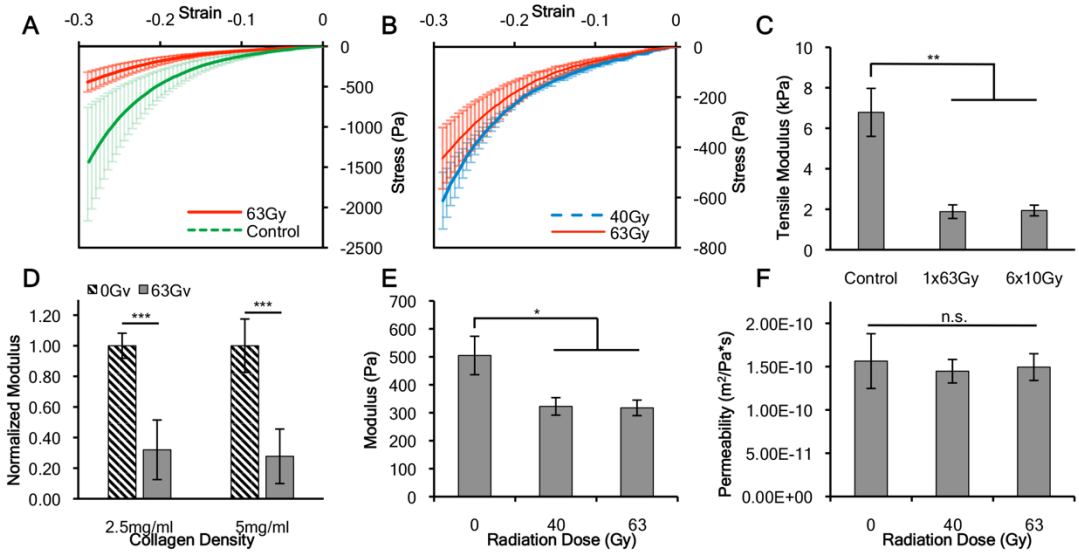

Fig 4.1: Ex vivo irradiated mammary tumors display mechanical differences. **A)** Stress/strain compression curves indicating a difference in slope (modulus) between tumors treated with 63Gy (Red, n=6) and untreated (Green, n=4). **B)** Stress/strain compression curve of tumors treated with 63Gy (Red, n=6) or 40Gy (Blue, n=2) showing a difference in slope (modulus). **C)** Tensile testing of *in vitro* collagen scaffolds revealed no difference between single fraction (1880.90Pa +/- 820.74Pa) or multi-fraction doses (1938.50Pa +/- 528.07Pa) (n=10, $^{**}p<0.01$) but significantly lower modulus compared to control (6784.85Pa +/- 3746.99). **D)** Normalized tensile modulus showing no significant density dependence between control (0Gy) and treatment (63Gy) in 2.5mg/mL (0.32 +/- 0.19) and 5mg/mL (0.28 +/- 0.18) ($p<0.001$). **E)** Compressive testing (n=10, $^{*}p<0.05$) showing a reduced modulus in the treatment groups (40Gy: 322.75Pa +/- 99.12Pa; 60Gy: 317.51Pa +/- 87.62Pa) compared to control (504.85Pa +/- 217.25Pa). **F)** Permeability (n=10) of the collagen scaffold following treatment showed no change.

4.2 Mechanical Testing of Irradiated 3D Collagen Scaffolds

Collagen is the most abundant protein in mammary tissue and indeed the whole body, and plays a critical role in the structural support of various tissues (116). Additionally, it has been shown that increased stiffness of the tumor ECM is due in large part to additional collagen deposition and increased crosslinking (37). The function of collagen, as well as its abundance, makes it the primary extracellular protein of interest in explaining the reduction of stiffness in the *ex vivo* mammary tumors (73). Thus, *in vitro*

PART I

3D collagen matrices were used to investigate the impact of the radiation on the mechanical and structural properties of collagen.

To assess the clinical potential for radiation to reduce ECM stiffness and further investigate the dose-dependent effects of radiation on ECM stiffness, a fractionated treatment schedule was employed on the collagen gels. Fractionated radiotherapy delivers a large total dose of radiation through consecutive, smaller doses separated by some amount of time. It is currently the standard of care for many cancer treatment plans (117). The tensile modulus of 5mg/mL collagen irradiated in a single fraction of 60Gy was compared to 6 doses of 10Gy separated by 24 hours and untreated gels. The modulus decreased in the collagen gels exposed to a single dose and those exposed to fractionated doses to an approximately equivalent level (Figure 4.1C). This result confirms the dose-dependent effect radiation has on the modulus of a collagen scaffold and suggests radiation-induced stiffness reduction may be accomplished using a more highly fractionated treatment plan.

To investigate whether the modulus reducing effect was dependent on collagen density, both 2.5mg/mL and 5mg/mL collagen gels were irradiated and underwent tensile testing. Data from each treatment group was normalized against its respective control group. The results indicate that the modulus of both densities of collagen were significantly decreased compared to their non-irradiated controls, however they were not significantly different from each other (Figure 4.1D). Thus, at least in the collagen density ranges most

relevant to breast cancer research (118), no significant density dependency on the modulus reducing effect of radiation is observed.

Collagen is a viscoelastic material and to be sure that there were no other changes in the mechanical properties which were not detectable using tensile testing alone, confined compression testing on 5mg/mL collagen gels irradiated at 40Gy and 63Gy was also performed. Again, the treatment groups showed a reduction in matrix stiffness compared to controls (Figure 4.1E). The difference between the treatment groups was not significant and less than the changes in tensile modulus relative to their control. This weaker response can be explained by noting the geometry of any given fiber in the matrix. With the small aspect ratio (diameter/length) of a collagen fiber, the stretching (tensile) mode will be significantly stiffer compared to compression, where the dominant fiber behavior will be bending (119).

To investigate whether radiation affects the porosity and microstructure of the collagen matrix, we investigated the permeability of the irradiated gels based on the outflow of liquid from the gel under step-wise compression. Importantly, no significant changes in permeability were detected (Figure 4.1F). Since the outflow is dominated by the porosity of the gel, the lack of difference between irradiated gels and controls implies an insignificant change in matrix architecture and that the softening of the collagen matrix is not simply due to destruction of the matrix.

To investigate the mechanism by which radiation decreases collagen stiffness, confocal reflectance microscopy was used to visualize collagen fiber architecture following radiation treatment. There were no significant architectural changes in gels before (Figure 4.2A) or after 63Gy of radiation (Figure 4.2B). To quantify the porosity of the matrix, autocorrelation studies on 'before' and 'after' confocal reflectance images were performed. The results indicate that radiation had no significant impact on the pore size of matrices (Figure 4.2C). This result supports the data indicating there were no significant differences in hydraulic permeability (Figure 4.1F); since the pores are the same size, the outflow remains unchanged. To determine whether any media or chemical diffusion differences were present in the treatment group, we performed a permeability assay using a FITC dye. The resulting diffusion curves show no significant differences in diffusion rates (Figure 4.2D). Together, these results indicate that radiation decreases matrix stiffness without altering matrix architecture.

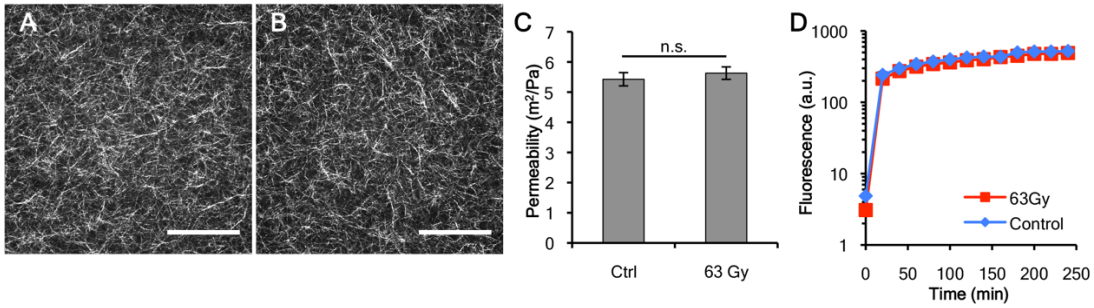

Fig. 4.2: Quantitative analysis of matrix architecture.
A) Confocal reflectance images before and after **(B)** irradiation. Scale bars are 150um **C)** Characteristic pore size determined by autocorrelation of control gels (5.43 +/- 1.26μm) and irradiated gels (5.63 +/- 1.13μm) (n=9). **D)** Permeability (Log-scale) of the FITC assay showing no significant change in the rate of diffusion between treatment and control gels (n=3).

4.3 Infrared Radiation Spectroscopy of Irradiated Collagen Scaffolds

After determining that radiation decreases the modulus of collagen without significantly altering its porosity or fiber organization, IR spectroscopy was utilized to investigate the mechanism by which the reduction occurs and to characterize the changes in the chemical landscape of the irradiated collagen.

IR spectra of irradiated versus control collagen gels (Figure 4.3) revealed a dramatic reduction in the 900-1200cm^{-1} fingerprint region indicating a lower presence of C-C, C-O and C-N bonds. The C-N and C-C bonds form the backbone of the collagen protein. The presence of both the 1640cm^{-1} Amide I and the 1550cm^{-1} Amide II regions, both of which are characteristic of the collagen spectra (120, 121), indicates that the collagen has not been denatured by the radiation. It is believed that the helical folding of collagen is stabilized by hydrogen bonds between the NH residues from peptide bonds of one chain and the carbonyl groups of an adjacent chain and this formation is enabled by the fixed angle of the C-N peptidyl-proline (120, 122). Thus, radiation-induced cleavage of these peptide bonds would destabilize the collagen triple helix by disrupting the helical primary structure. When a sufficient number of bonds are broken, any stiffness increase from crosslinked fibers must be overwhelmed and a net reduction in the bulk modulus occurs, supporting our mechanical testing measurements.

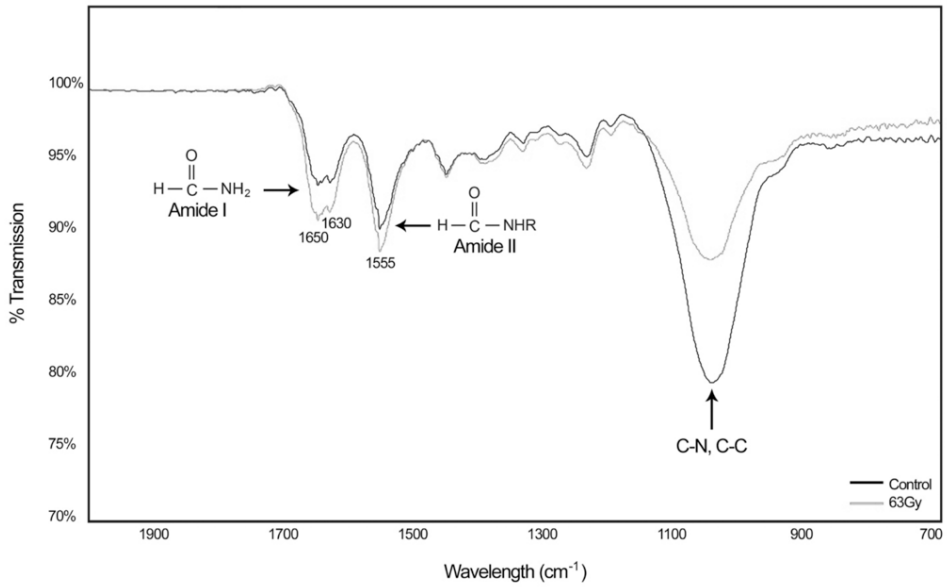

Fig. 4.3: IR spectra of irradiated and control collagen.
Irradiated collagen matrices show a reduction in the 900-1200cm^{-1} region indicating a reduced number of C-C and C-N bonds. The presence of Amide groups I and II indicate the collagen helix has not been denatured.

4.4 Cell Adhesion and Spreading on Irradiated Collagen Scaffolds

Having established that radiation reduces stiffness in collagen without altering fiber architecture, the question of whether cells respond to radiation-softened matrix as predicted by previous literature (22,24) was investigated. Specifically, highly metastatic MDA-MB-231 cancer cells were seeded on irradiated collagen gels, and were monitored for adhesion, spreading, and invasion.

Over a 60min period, cells exhibited a reduced capacity for adhesion to irradiated collagen compared to controls (Figure 4.4A, B, C). Investigating cell spreading over time revealed the same trend. Cells that were seeded on the less stiff, irradiated matrices exhibited difficulty with initial spreading. After 30min, they appeared to continue

spreading at a lower rate, and occupied consistently smaller areas throughout the 2hrs window within which they were observed (Figure 4.4D).

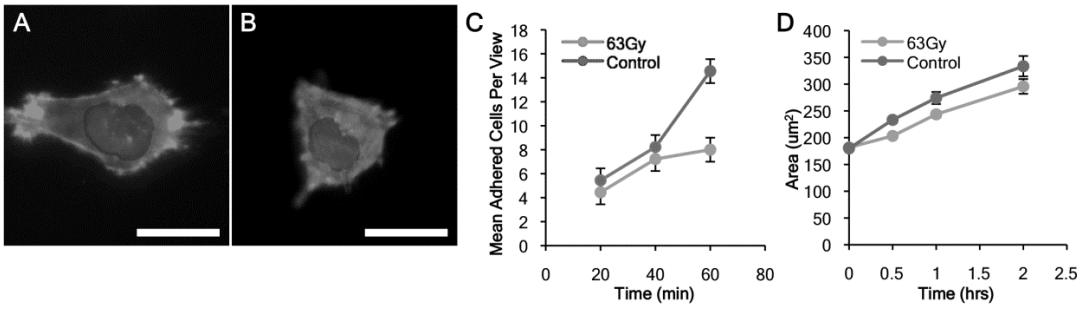

Fig. 4.4: Cell adhesion over time.
A) Fluorescent image of representative cell on control gels **(B)** compared to cells on irradiated gels at 2hrs post-plating. Scale bar = 20um. **C)** MDA-MB-231 cells exhibited a reduced capacity to adhere to irradiated collagen gels (n=354 586) compared to controls at 60min (n=508). **D)** Cell rate of spreading is also reduced on the softer irradiated collagen gels (n=586) compared to controls (n=451) (Control Cell Area=75.20t, R^2=0.98; Irradiated Cell Area=58.44t, R^2=0.99) (n=6).

4.5 Cancer Cell Invasion in Irradiated Collagen Scaffolds

To determine the effects of ECM-targeted radiation on metastatic cell invasion, a transwell invasion assay was performed (Figure 4.5A). After 7 days, fewer cells invaded through the irradiated collagen gels compared to untreated gels, consistent with behavior of cells in less stiff collagen (64). Further, after 2 days of additional invasion, consistently fewer cells were capable of traversing the matrix as revealed with fluorescent images of DAPI stained cells (Figure 4.5B, C, D).

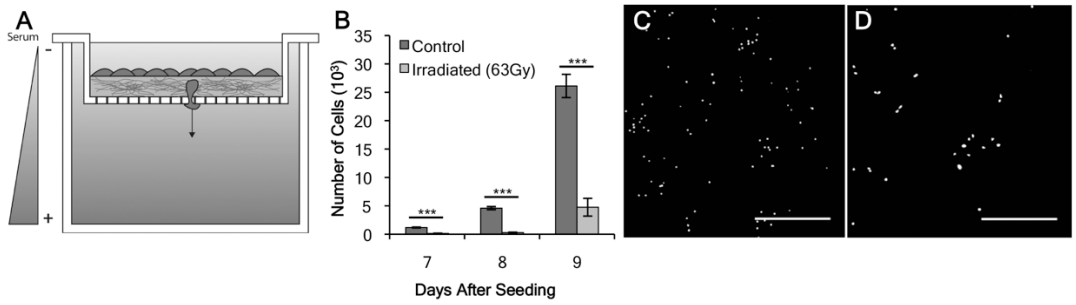

Fig. 4.5: Cell invasion over time.
A) Transwell invasion schematic with serum gradient conditions. Cells are seeded on 500μm of 2.5mg/mL collagen and allowed to invade through the matrix and pass through 8 μm pores. **B)** Invasion results indicating cells invade through irradiated collagen at a persistently lower rate compared to controls. (n=6) Representative fluorescent images (DAPI) of invaded cells through control gels **(C)** and irradiated gels **(D)**. Scale bars are 150um.

4.6 Further Discussion and Conclusion

The work described here indicates that clinical doses of radiation alter the mechanical properties of the ECM. Radiation dramatically reduced the compressive modulus of an *ex vivo* mammary tumor. Further investigation of the principle matrix protein, collagen, revealed that this reduction of stiffness occurs without significant alterations to the architecture of the 3D collagen scaffold, as shown using confocal reflectance microscopy, permeability measurements during compression testing, and a dye-diffusion permeability assay. Further, IR spectroscopy confirmed that radiation does not denature the collagen, and revealed the reduction in stiffness occurs due to the cleaving of C-C and C-N peptide bonds in the backbone of the collagen protein. To determine whether these mechanical changes in the extracellular matrix impact cell behavior, highly metastatic MDA-MB-231 mammalian breast cancer cells were seeded in irradiated collagen gels. Cells in irradiated gels exhibited a reduction in the rate of cell adhesion, the capacity for cells to spread, and most importantly, the invasiveness of cells through the collagen. Overall, these results

demonstrate that radiation treatment can effectively lower matrix stiffness through its destabilizing effects on the collagen structure which in turn affects metastatic cell behavior.

Currently, there is no clinical mechanism aimed at correcting the increased stiffness in the ECM, a hallmark of the tumor microenvironment (18). However, if levels of radiation can be identified that minimize cytotoxic effects, but reduce ECM stiffness through hyperfractionated treatment planning, the potential for applications of radiation with fewer side effects and longer-lasting benefits exist. In this report, we show that clinical levels of radiation have a stiffness-reducing effect on the ECM in a dose-dependent manner. Even more encouraging, the results are applicable to the common fractionated treatment strategy used clinically. Fractionated radiotherapy is a common technique because it allows time for healthy cells to repair radiation damage from a small dose, while cancerous cells often have mutations that make them less efficient in their repair processes (98). This allows the cumulative effects of the treatment to be more damaging to cancerous cells than to the patient's healthy cells (117, 123, 124). Expanding our knowledge to include the effects of radiation on the mechanical properties of tissue and how cells respond to those properties opens the door to potentially realize additional benefits from current standards of care.

Importantly, our results may help to explain the results of the EORTC trial (115) and others (110–112, 125) like it where additional radiation has a cancer controlling effect and a reduction in the rate of recurrence. Indeed, our data align and support the many

recent research findings that ECM mechanical properties, such as stiffness, play a critical role in the determination of a cell's malignant capacity (33, 38). Further, it has been shown that stiffness alone can promote a cancerous phenotype (2, 22, 126). Thus, radiation therapy is uniquely positioned as a potential therapy used to mitigate the increased stiffening of the local tumor environment known to correlate with poor patient outcomes (9, 127, 128).

It is well appreciated that cells of various types can respond to radiotherapy with varying results (129). The mechanobiological effects of radiation discussed here suggest a potential explanation as to why some cell lines may be more radioresistant than others or why certain treatment plans have more or less favorable outcomes in terms of recurrence. In light of this work, our data suggests that the effects of radiation on the mechanical properties of the microenvironment may have a significant impact on the net outcome of a radiation treatment plan. Indeed, it has been shown that cancer cells can be sensitized to various drugs by altering the stiffness of the ECM (38, 130, 131). Therefore, these data suggest that in addition to understanding how cells of various types respond to radiation directly, we must also investigate how cells respond to the mechanical changes within their environment brought on by the irradiation of the ECM. The latter effect very well may prove to be a principle component in determining patient outcome.

Currently, radiotherapy has been used almost exclusively for targeted cell death. The data reported here supports an expanded role for radiotherapy in the targeting of the ECM for the purpose of reducing matrix stiffness and intentionally altering the biomechanics of the

cellular microenvironment. Nearly half of all cancer diagnoses in the United States are accompanied with a treatment plan that includes radiotherapy (132). With the clinical pervasiveness of such a tool, it is exciting to find that radiation alters tissue biomechanics in a way that may positively impact long-term patient outcomes. With reports already confirming that cancer recurrence is reduced in patients who receive additional radiation, a strategy of follow-up, fractionated radiation dosing following initial treatment may be a promising path to reducing recurrence by reducing ECM stiffness.

CHAPTER 5

Future Directions and Concluding Remarks

The data presented in this thesis thus far has argued that the cell-ECM dyanmic is directed by various mechanical cues including ECM density, alignment, stiffness and tension and done so under the umbrella of energy expenditure. However, there are additional mechanical properties that have been neglected.

The time dependent response of a viscoelastic material such as collagen is a critical mechanical property only recently being explored by mechanobiologists. In the previous chapters, a purely elastic model was used in order to simplify the complexity. To form a more complete model, the theoretical treatment must also include the relaxation and strain stiffening that occurs as a function of power, which is the force divided by the time the force is applied. Collagen exhibits a stiffening as the strain or power exerted upon it increases. Further, once strained, the collagen exhibits relaxation if no additional force is applied. This behavior is typically modelled as an elastic spring in parallel with a Newtonian dashpot. Mathematically, this is equivalent to including a first order, linear term into the characteristic equation. To complicate things further, one may imagine this force oscillating as a function of time. To model all of this behavior, one must solve an equation of the form:

$$\frac{d^2x}{dt^2} + \lambda\frac{dx}{dt} + w^2x = G(x,t)$$

Indeed, the velocity and the driving force term may be highly nonlinear *in vivo*.

The largest barrier to be surmounted with respect to this more complete model of the ECM is developing *in vitro* systems capable of controlling for the previously discussed mechanical properties (alignment, tension, etc.) and at the same time controlling a well-defined $G(x,t)$ in order to understand the frequency response of the matrix (w^2) and cell-ECM dynamic. One of the more novel approaches is to reduce the dimensionality of the matrix to a single fiber, which is instead of 3D systems, develop 1D systems. In a single fiber system, alignment is perfectly defined, tension can be perfectly defined, density does not exist and most critically, the driving force can be controlled and experimented upon. The challenge then is to produce a single fiber in which a cell can attach and respond; to this end, electrospinning is a promising method.

5.1 A Cell in Lineland

The established models for cell motility have been formulated in large part from 2D cell studies (133–135). The basic cell dynamics in 2D can be summarized in four steps (35): protrusion at the leading edge (actin-rich lamellipodia), adhesion, cell body translocation and finally, retraction of the trailing edge. A cell's capacity for migration depends on the synchronization and ability to perform each of these functions. However, when tools developed to support more detailed studies of cell motility in 3D, Petrie et al. (136) discovered that cells have an additional mode of motility, which they can readily switch to in response to the degree of polarity and mechanical properties sensed in the surrounding extracellular matrix (ECM) (137). In contrast to 2D motility, this second mode does not involve the extensions of thin, fan-

shaped lamellipodia but instead found to be cylindrical, blunt lobopodia driven by intracellular pressure. Further, cell staining revealed it lacked the rich polymerization of actin characteristic of lamellipodia motility (138). Research has since gone a step further and found that by modifying only the elastic properties of the matrix, one could induce the cells to switch between the two modes of motility (137, 139, 140).

1D matrices have been largely unexplored. However, Doyle et al have published a surprising finding: cell motility in a 1D micro-patterned architecture is in closer agreement with observed 3D motility (138). In their experiment, they coat glass slides with a polyvinyl alcohol (PVA) coat, which is strongly hydrophobic and prevents cell and protein adhesion. Next, they create a micro pattern on the surface using 2-photon ablation. At this point, proteins may be added to the pattern and adhere to the ablated areas. Serializing this process allows for micro patterning of different proteins. The results of their experiments with this technique revealed that ECM topography could regulate cell migration rate, and cell phenotype regardless of ligand density. Further, they found 1D cell networks of microtubules and actomyosin regulation corresponded with what is observed in 3D migration (141).

It has been shown that alignment within an ECM can polarize a cell and direct its migration in metastatic models (80) and during embryonic development (142). In addition, polarity and migration are moderated by matrix stiffness (143). Thus, it is a natural extension to investigate the role of stiffness in 1D environments. To do this, we must have an ability to form a single detached fiber from the substrate surface.

Further, we must be able to activate this fiber to modulate stiffness. Ideally, the solution would be reversible with minimal hysteresis and appear chemically native to the cell.

As an early test of this capability, coaxially spun polyvinylidene difluoride (PVDF) inside a sheath of Type I Rat Tail Collagen was produced. PVDF is a polymer that forms a permanent dipole moment orthogonal to the fiber axis when exposed to a high electric field. In the natural course of electrospinning, such a field is applied and PVDF becomes permanently piezoelectric. By coaxially spinning collagen on the outside of the PVDF, any cell exposed to the fiber "sees" a native structure. If we then electrospin the coaxial fiber over a pillar-pattered glass slide coated with Indium-Tin-Oxide (ITO), and "sandwich" the matrix with another ITO slide, we have what is essentially a parallel plate system. If we then attach electrodes to these slides and apply a small voltage (0-20V), we can modulate the stiffness in the PVDF and therefore the fibers.

One interesting future direction is to investigate the nature of cell-cell communication in 1D and how ECM stiffness may affect it? In this case, the metaphor of two cells speaking through a taut wire may be appropriate. The distance at which two cells can communicate mechanically should increase with increased stiffness.

If first experiment would be to place two cells on one fiber and see what distance they typically begin to come together. The second experiment would be to vary the

stiffness of the fiber and see how that affects the distance two cells will begin to come together.

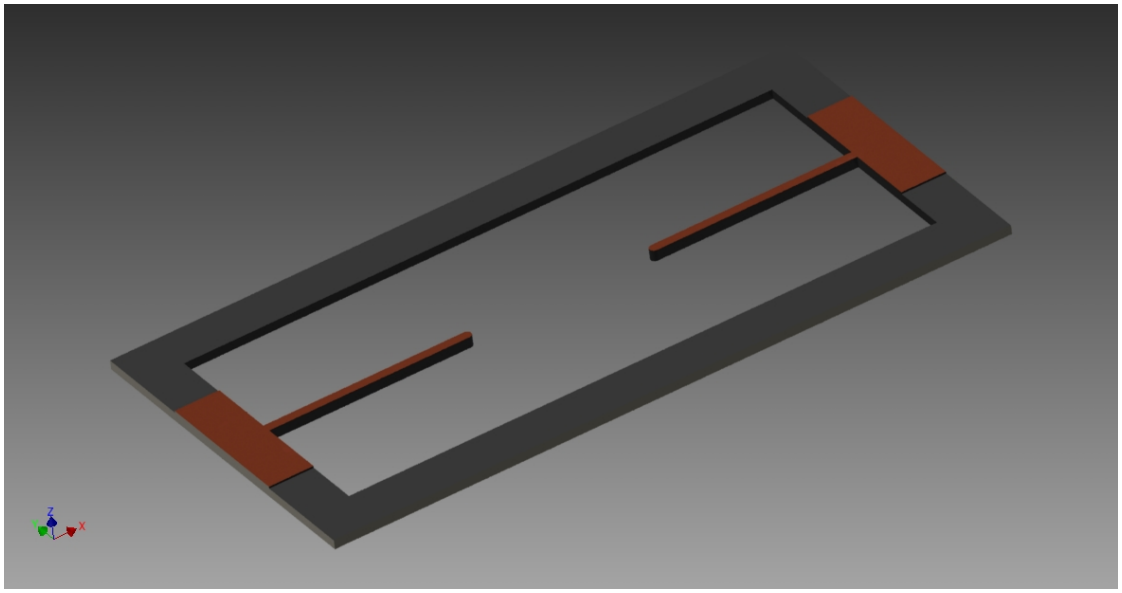

Figure 1 – Hypothetical device for 1-D activation of PVDF-Collagen fiber.

5.2 Active Scaffolds

The ability to mimic the relevant ECM in cell behavior studies has become increasingly important. This is particularly so in cancer research where it has been shown increased cross-linking and a stiffening of the ECM accompanies tumorigenesis (75). Further, many other studies have confirmed mechanical cues from the surrounding environment influence apoptosis (144), proliferation (145), differentiation (146), and can polarize cells to migrate (147).

While it's now clear that physical properties of the ECM are playing a significant role in cell behavior, it is less certain which of these properties and to what level of

influence it might have on a particular decision made by the cell. To get at this question, many cleverly engineered scaffolds have been invented capable of isolating various mechanical properties (148). Each has made an important contribution to understanding cell behavior by allowing investigators to "tune" the environment in which the cell exists and observe behavior as a result. While all of scaffold designs have certain advantages, each also comes with its own set of trade-offs.

Naturally derived hydrogels are amongst the most popular engineered scaffolds for a number of reasons. First, they are built using the critical ECM components seen in native tissue. Specifically, type I collagen, fibrin and hyaluronic acid (HA) (149–151). Because of this native composition, cells actively degrade and remodel this environment. This has become an increasingly important feature for any engineered scaffold. Recent research has shown cells actively respond to mechanical cues by remodeling their ECM. Further, a stress-sensing cell can recruit another cell type to undergo remodeling of the matrix in order to maintain homeostasis (152). Thus, not only can remodeling be a direct result of mechanical stress on a cell, but it can also be the feedback from cell-cell communication induced by mechanical stress on a cell. Finally, naturally derived hydrogels have a fairly straightforward relationship with component density to matrix stiffness. For example, in collagen it has been shown a density increase from 2 mg/ml to 20mg/ml results in a modulus increase from 175 Pa to 1800 Pa (150). To an even greater extent, an increase in fibrin density from 2.5mg/ml to 10mg/ml resulted in a modulus increase from 1.3kPa to 9kPa (152). Further, in a two-step cross-linking technique, methylacrylated HA has been designed

with a modulus of 1.5kPa and then photo-cross-linked to dynamically increase the modulus to 7.5kPa (153). The temporality of this latter technique aims at the dynamic requirements future engineered scaffolds must be able to meet. Despite its many advantages, naturally derived hydrogels are not without their trade-offs. For example, methylacrylated HA are not naturally porous so other means of creating these pores are introduced and result in a less topologically relevant model. Further, these gels convolute the matrix density and therefore stiffness with adhesion site availability and care must be taken when ascribing cell behavior to the result of stiffness or an increase in adhesion.

To overcome these trade-offs, synthetic gels provide some relief. Synthetic gels offer independent control of many mechanical properties, the binding site density and can be tuned to present an appropriate chemical environment to the cell. Additionally, Poly-ethylene glycol (PEG) gels have been shown to function with MMP-sensitive cross-links, which allow cells to actively degrade the matrix (154–157). However, these synthetic cells are typically not fibrous ECM and while cells may degrade the synthetic matrix, they do not actively remodel it as they would in the body.

Mixed-matrices attempt to blend different components to capture both tunable properties and more native composition. However, again, this mixture of materials convolutes the signals driving cell behavior.

Collagen glycation has the advantage of being tunable in stiffness while not affecting the fibrous architecture (153). Because the matrix is composed with native materials, cells will actively degrade and remodel the matrix. The disadvantage in this technique is that the process chemically alters the matrix by creating advanced glycation end-products (AGE), which have been shown to interact with receptors on a cells plasma membrane (RAGE) and up-regulate erg-1 expression. This is a pathway characteristically active in a number of common diseases such as diabetes, aging, renal failure, inflammation and hypoxia (158).

Electrospinning's primary advantage is its ability to produce fibrous scaffolds of natural, synthetic or mixed components. As a result, porosity, stiffness, fiber architecture, adhesion site density and chemical makeup can be controlled with impressive precision (159). Hollow, coaxial or even tri-axial spun fibers have the ability to transport growth factors inside a sheath, deliver inhibitory drugs with controlled diffusion or form multicomponent fibers. Additionally, electrospun fibers can be aligned or patterned to form organized topologies. However historically, once a scaffold has been spun lacks the ability for dynamic change.

The novel polyvinylidene difluoride or PVDF-based scaffold described previously maybe capable of undergoing dynamic and reversible changes in density and stiffness, while maintaining the native properties of a biologically relevant material for cell interaction. Table 1 summarizes the capabilities of the various matrices and the potential of the PVDF based scaffold.

Table 1 – Summary of controllable mechanical properties

	Cells Remodel	Tunable Stiffness	Native Chemistry	Controlled Fiber Architecture	Controllable Pore Size	Independent Control of Properties
Natural Hydrogels	Yes	Limited	Yes	Yes	Limited	No
Synthetic Hydrogels	Limited	Yes	Yes	No	Limited	Yes
Mixed Matrices	Limited	Yes	Yes	Yes	Yes	Limited
Collagen Glycation	Yes	Limited	Limited	Yes	Yes	Limited
PVDF-Based ES.	Unknown	Yes	Yes	Yes	Yes	Yes

5.3 Final Thoughts

Cells, like all systems, must operate within the confines of thermodynamics. No system, biological or otherwise, produces more energy than it consumes. Therefore, as progressively complex tasks increase their demand for energy, energy becomes a scares resource. Yet biological systems have evolved to produce enormously complex tasks requiring the syncopation of literally millions of processes. How did these systems come to be so efficient with the limited resources available? We may infer that systems capable of performing any task with the least energy are more dynamic, efficient and energetically capable of responding to increasingly complex signals than those that expend more energy less efficiently and thus have less energy in which to respond to deviations from homeostasis. In this sense, thermodynamic efficiency may be thought of as a byproduct of the natural evolutionary process. This is the primary logic behind the work presented in this dissertation.

Expanding upon this line of reasoning, one may imagine that the landscape of available energy for cells is fixed by natural boundaries. These boundaries include variables such as the rate limiting steps of glycolysis or various protein productions, the maximum torque generated in the electrodynamics of a phosphorylated myosin motor or any number of the mechanical properties of the ECM. As density increases, porosity shrinks and this limits the cells capacity for migration. As fiber stiffness is reduced, collagen fibers become too elastic and no translocation can occur. In any given microenvironment, a cell's boundary conditions are defined by the set of all the aforementioned variables and others yet to be defined. However, it's reasonable to suggest that during healthy homeostasis, a cell in its native tissue is optimally functional given the boundary conditions of that healthy tissue. Indeed, this optimality may be the very bedrock of homeostasis. Yet, as health is reduced due to the introduction of toxins, lack of exercise, poor eating habits that alter mechanical properties of the ECM or simply the passage of time, these boundary conditions change and the cells that were once optimal in their environment find themselves increasingly suboptimal. At the same time, the natural heterogeneity of the cell population in any given tissue triggers some subpopulation of the cells to behave differently, perhaps more optimally given the new boundary conditions, and selection becomes a force within the population. In some cases, it's possible, these cells may behave in a manner characteristic of cancer. Invasive behavior may be reimagined as a subpopulation looking to reestablish optimality by migrating to different conditions, either due to genetic mutation or in response to the boundary changes that result from the work of those genetically identified as cancer. Indeed, a number of observations in

cancer cell behavior of various tissues, including questions such as: “why do cells that metastasize from one tissue appear to prefer particular other tissues to invade?”; “Do boundaries play a role in inducing endothelial to mesenchymal transitions?”, and “Do the strengths and weaknesses of the various cells in heterogeneous populations determine metastatic potential?”. Dr. Robert Austin once remarked during a keynote address that the solution to cancer may be more cancer. It was received as being only half serious at the time but ironically, in light of Dr. William Bialek’s work on optimization theory, it’s very possible that the solution to cancer is to have another cancer compete for resources. Since cancer cells are particularly competitive for resources as it is, we may find that borrowing a strategy from economics is the appropriate treatment: to break up monopolies, you must inject competition. This results in a reallocation of resources such that no single competitor can define the market.

In conclusion, this dissertation has attempted to ground, at least in part, the vast complexity of cancer cell biology by presenting data indicating cells respond to mechanical properties within their microenvironment not as single independent cues, but for the purpose of minimizing the energy expenditure necessary to carry out a task such as invasion. This energy minimizing principle is powerful and through already existing technology such as radiotherapy, one may increase the energy required by invading cells thereby reducing their metastatic potential.

REFERENCES

1. Provenzano, P.P., D.R. Inman, K.W. Eliceiri, S.M. Trier, and P.J. Keely. 2008. Contact guidance mediated three-dimensional cell migration is regulated by Rho/ROCK-dependent matrix reorganization. Biophys. J. 95: 5374–5384.
2. Hadjipanayi, E., V. Mudera, and R.A. Brown. 2009. Guiding cell migration in 3D: A collagen matrix with graded directional stiffness. Cell Motil. Cytoskeleton. 66: 121–128.
3. Bordeleau, F., L.N. Tang, and C.A. Reinhart-King. 2013. Topographical guidance of 3D tumor cell migration at an interface of collagen densities. Phys. Biol. 10: 065004.
4. Ma, X., M.E. Schickel, M.D. Stevenson, A.L. Sarang-Sieminski, K.J. Gooch, S.N. Ghadiali, and R.T. Hart. 2013. Fibers in the extracellular matrix enable long-range stress transmission between cells. Biophys. J. 104: 1410–1418.
5. Théry, M. 2010. Micropatterning as a tool to decipher cell morphogenesis and functions. J. Cell Sci. 123: 4201–13.
6. Chen, C.S., M. Mrksich, S. Huang, G.M. Whitesides, and D.E. Ingber. 1997. Geometric Control of Cell Life and Death. Science (80-.). 276: 1425–1428.
7. Kilian, K. a, B. Bugarija, B.T. Lahn, and M. Mrksich. 2010. Geometric cues for directing the differentiation of mesenchymal stem cells. Proc. Natl. Acad. Sci. U. S. A. 107: 4872–7.
8. Chen, B., G. Kumar, C.C. Co, and C.-C. Ho. 2013. Geometric control of cell migration. Sci. Rep. 3: 2827.
9. Pickup, M.W., J.K. Mouw, and V.M. Weaver. 2014. The extracellular matrix modulates the hallmarks of cancer. EMBO Rep. 15: 1243–1253.
10. Yang, C., F.W. DelRio, H. Ma, A.R. Killaars, L.P. Basta, K.A. Kyburz, and K.S. Anseth. 2016. Spatially patterned matrix elasticity directs stem cell fate. Proc. Natl. Acad. Sci. : 201609731.
11. Ahmad, A. 2013. Pathways to breast cancer recurrence. ISRN Oncol. 2013: 290568.
12. Kai, F.B., H. Laklai, and V.M. Weaver. 2016. Force Matters: Biomechanical Regulation of Cell Invasion and Migration in Disease. Trends Cell Biol. 26: 486–497.
13. Rahman, A., S.P. Carey, C.M. Kraning-Rush, Z.E. Goldblatt, F. Bordeleau, M.C. Lampi, D.Y. Lin, A.J. Garcia, and C.A. Reinhart-King. 2016. Vinculin regulates directionality and cell polarity in two- and three-dimensional matrix and three-dimensional microtrack migration. Mol. Biol. Cell. 27: 1431–1441.
14. Dos Remedios, C.G., D. Chhabra, M. Kekic, I. V Dedova, M. Tsubakihara, D.A. Berry, and N.J. Nosworthy. 2003. Actin binding proteins: Regulation of cytoskeletal microfilaments. Physiol Rev. 83: 433–473.
15. Orr, A.W., B.P. Helmke, B.R. Blackman, and M.A. Schwartz. 2006. Mechanisms of mechanotransduction. Dev. Cell. 10: 11–20.
16. Paszek, M.J., N. Zahir, K.R. Johnson, J.N. Lakins, G.I. Rozenberg, A. Gefen, C.A. Reinhart-King, S.S. Margulies, M. Dembo, D. Boettiger, D.A. Hammer, and V.M. Weaver. 2005. Tensional homeostasis and the malignant phenotype.

Cancer Cell. 8: 241–54.
17. Prockop, D., K. Kivirikki, L. Tuderman, and N. Guzman. 1979. The Biosynthesis of collagen and its disorders. N. Engl. J. Med. 301: 13–23.
18. Carey, S.P., A. Rahman, C.M. Kraning-Rush, B. Romero, S. Somasegar, O.M. Torre, R.M. Williams, and C.A. Reinhart-King. 2014. Comparative mechanisms of cancer cell migration through 3D matrix and physiological microtracks. AJP Cell Physiol. 308: C436-47.
19. Bordeleau, F., T. a Alcoser, and C. a Reinhart-King. 2014. Physical biology in cancer. 5. The rocky road of metastasis: the role of cytoskeletal mechanics in cell migratory response to 3D matrix topography. Am. J. Physiol. Physiol. 306: C110-20.
20. Lake, S.P., K.S. Miller, D.M. Elliott, and L.J. Soslowsky. 2010. Effect of fiber distribution and realignment on the nonlinear and inhomogeneous mechanical properties of human supraspinatus tendon under longitudinal tensile loading. J. Orthop. Res. 27: 1–17.
21. Chaudhuri, O., S.T. Koshy, C. Branco da Cunha, J.-W. Shin, C.S. Verbeke, K.H. Allison, and D.J. Mooney. 2014. Extracellular matrix stiffness and composition jointly regulate the induction of malignant phenotypes in mammary epithelium. Nat. Mater. 13: 1–35.
22. Carey, S.P., C.M. Kraning-Rush, R.M. Williams, and C.A. Reinhart-King. 2012. Biophysical control of invasive tumor cell behavior by extracellular matrix microarchitecture. Biomaterials. 33: 4157–4165.
23. Kraning-Rush, C.M. 2013. Microfabricated collagen tracks facilitate single cell metastatic invasion in 3D. Integr Biol. 18: 1199–1216.
24. Ronceray, P., C. Broedersz, and M. Lenz. 2016. Fiber networks amplify active stress. PNAS. 113: 2827–2832.
25. Wang, H., A.S. Abhilash, C.S. Chen, R.G. Wells, and V.B. Shenoy. 2014. Long-Range Force Transmission in Fibrous Matrices Enabled by Tension-Driven Alignment of Fibers. Biophysj. 107: 2592–2603.
26. Karamichos, D., J. Skinner, R. Brown, and V. Mudera. 208AD. Matrix stiffness and serum concentration effects matrix remodelling and ECM regulatory genes of human bone marrow stem cells. J. Tissue Eng. Regen. Med. 2: 97–105.
27. Zhang, Y.H., C.Q. Zhao, L.S. Jiang, and L.Y. Dai. 2011. Substrate stiffness regulates apoptosis and the mRNA expression of extracellular matrix regulatory genes in the rat annular cells. Matrix Biol. 30: 135–144.
28. Okada, M., A. Matsumori, K. Ono, Y. Furukawa, T. Shioi, A. Iwasaki, K. Matsushima, and S. Sasayama. 1998. Cyclic Stretch Upregulates Production of Interleukin-8 and Monocyte Chemotactic and Activating Factor / Monocyte Chemoattractant Protein-1 in Human Endothelial Cells. Arter. Thromb Vasc Biol. 18: 894–901.
29. Yokoyama, T., K. Sekiguchi, T. Tanaka, K. Tomaru, M. Arai, T. Suzuki, and R. Nagai. 1999. Angiotensin II and mechanical stretch induce production of tumor necrosis factor in cardiac fibroblasts. Am. J. Physiol. 276: H1968–H1976.
30. Liotta, L. a, and E.C. Kohn. 2001. The microenvironment of the tumour-host interface. Nature. 411: 375–379.

31. Shi, Q., R.P. Ghosh, H. Engelke, C.H. Rycroft, L. Cassereau, J.A. Sethian, V.M. Weaver, and J.T. Liphardt. 2014. Rapid disorganization of mechanically interacting systems of mammary acini. Proc. Natl. Acad. Sci. U. S. A. 111: 658–63.
32. Liu, L., G. Duclos, B. Sun, J. Lee, A. Wu, Y. Kam, E.D. Sontag, H. a Stone, J.C. Sturm, R.A. Gatenby, and R.H. Austin. 2013. Minimization of thermodynamic costs in cancer cell invasion. Proc. Natl. Acad. Sci. U. S. A. 110: 1686–91.
33. Hanahan, D., and R.A. Weinberg. 2011. Hallmarks of cancer: The next generation. Cell. 144: 646–674.
34. Stevens, M.M., and J.H. George. 2005. Exploring and engineering the cell surface interface. Science. 310: 1135–1138.
35. Ridley, A.J., M.A. Schwartz, K. Burridge, R.A. Firtel, M.H. Ginsberg, G. Borisy, J.T. Parsons, and A.R. Horwitz. 2003. Cell Migration: Integrating Signals from Front to Back. Science. 302: 1704–1709.
36. Petrie, R.J., A.D. Doyle, and K.M. Yamada. 2010. Random versus directionally persistent cell migration. Mol. Cell. 10: 538–549.
37. Carey, S.P., T.M. D'Alfonso, S.J. Shin, and C. a Reinhart-King. 2012. Mechanobiology of tumor invasion: engineering meets oncology. Crit. Rev. Oncol. Hematol. 83: 170–83.
38. Lu, P., V.M. Weaver, and Z. Werb. 2012. The extracellular matrix: A dynamic niche in cancer progression. J. Cell Biol. 196: 395–406.
39. Gao, D., L.T. Vahdat, S. Wong, J.C. Chang, and V. Mittal. 2012. Microenvironmental regulation of epithelial-mesenchymal transitionsin cancer. Cancer Res. 72: 4883–4889.
40. Polacheck, W.J., I.K. Zervantonakis, and R.D. Kamm. 2013. Tumor cell migration in complex microenvironments. Cell. Mol. Life Sci. 70: 1335–1356.
41. Kalluri, R., and R.A. Weinberg. 2009. The basics of epithelial-mesenchymal transition. J. Clin. Invest. 119: 1420–1428.
42. Zavadil, J., J. Haley, R. Kalluri, S.K. Muthuswamy, and E. Thompson. 2008. Epithelial-Mesenchymal Transition. Cancer Res. 68: 9574–9577.
43. Ingber, D.E. 2008. Can cancer be reversed by engineering the tumor microenvironment? Semin. Cancer Biol. 18: 356–364.
44. Van Horssen, R., E. Janssen, W. Peters, L. Van de Pasch, M.M. Te Lindert, M.M.T. Van Dommelen, P.C. Linssen, T.L.M. Ten Hagen, J.A.M. Fransen, and B. Wieringa. 2009. Modulation of cell motility by spatial repositioning of enzymatic ATP/ADP Exchange capacity. J. Biol. Chem. 284: 1620–1627.
45. Yuan, H.-X., Y. Xiong, and K.-L. Guan. 2014. Nutrient sensing, metabolim, and cell growth control. Mol. Biol. Rep. 49: 379–387.
46. Chen, E.I., J. Hewel, J.S. Krueger, C. Tiraby, M.R. Weber, A. Kralli, K. Becker, J.R. Yates, and B. Felding-Habermann. 2007. Adaptation of energy metabolism in breast cancer brain metastases. Cancer Res. 67: 1472–1486.
47. Caneba, C.A., N. Bellance, L. Yang, L. Pabst, and D. Nagrath. 2012. Pyruvate uptake is increased in highly invasive ovarian cancer cells under anoikis conditions for anaplerosis, mitochondrial function, and migration. AJP

Endocrinol. Metab. 303: E1036–E1052.
48. Alberts, B., A. Johnson, and J. Lewish. 2002. Molecular Biology of the Cell. 4th edition. 4th ed. New York: Garland Science.
49. Bergman, J. 1999. ATP: The Perfect Energy Currency for the Cell. Creat. Res. Soc. Q. 36.
50. Kennedy, H.J., A.E. Pouli, E.K. Ainscow, L.S. Jouaville, R. Rizzuto, and G.A. Rutter. 1999. Glucose generates sub-plasma membrane ATP microdomains in single islet ß-cells. J. Biol. Chem. 274: 13281–13291.
51. Yaniv, Y., H.A. Spurgeon, B.D. Ziman, A.E. Lyashkov, and E.G. Lakatta. 2013. Mechanisms that match ATP supply to demand in cardiac pacemaker cells during high ATP demand. Am J Physiol Hear. Circ Physiol. 304: H1428-38.
52. Uslu, V. V, and G. Grossmann. 2016. The biosensor toolbox for plant developmental biology. Curr. Opin. Plant Biol. 29: 138–147.
53. Merrins, M.J., C. Poudel, J.P. McKenna, J. Ha, A. Sherman, R. Bertram, and L.S. Satin. 2016. Phase Analysis of Metabolic Oscillations and Membrane Potential in Pancreatic Islet β-Cells. Biophys. J. 110: 691–699.
54. Thomas, S., and D.A. Fell. 1998. A control analysis exploration of the role of ATP utilisation in glycolytic-flux control and glycolytic-metabolite-concentration regulation. Eur. J. Biochem. 258: 956–967.
55. Imamura, H., K.P.H. Nhat, H. Togawa, K. Saito, R. Iino, Y. Kato-Yamada, T. Nagai, and H. Noji. 2009. Visualization of ATP levels inside single living cells with fluorescence resonance energy transfer-based genetically encoded indicators. Proc. Natl. Acad. Sci. U. S. A. 106: 15651–6.
56. Wu, M., A. Neilson, A.L. Swift, R. Moran, J. Tamagnine, D. Parslow, S. Armistead, K. Lemire, J. Orrell, J. Teich, S. Chomicz, and D. a Ferrick. 2007. Multiparameter metabolic analysis reveals a close link between attenuated mitochondrial bioenergetic function and enhanced glycolysis dependency in human tumor cells. Am. J. Physiol. Cell Physiol. 292: C125-36.
57. Hyslop, P.A., D.B. Hinshaw, W.A. Halsey, I.U. Schraufstatter, R.D. Sauerheber, R.G. Spragg, J.H. Jackson, and C.G. Cochrane. 1988. Mechanisms of oxidant-mediated cell injury. The glycolytic and mitochondrial pathways of ADP phosphorylation are major intracellular targets inactivated by hydrogen peroxide. J. Biol. Chem. 263: 1665–1675.
58. Tarasov, A.I., and G.A. Rutter. 2014. Use of genetically encoded sensors to monitor cytosolic ATP/ADP ratio in living cells. 1st ed. Elsevier Inc.
59. Berg, J., Y. Pun Hung, and G. Yellen. 2009. A genetically encoded fluorescent reporter of ATP/ADP ratio. Nat Methods. 6: 161–166.
60. Wheaton, W.W., and N.S. Chandel. 2011. Hypoxia. 2. Hypoxia regulates cellular metabolism. Am. J. Physiol. Cell Physiol. 300: C385–C393.
61. Tantama, M., J.R. Martínez-françois, R. Mongeon, and G. Yellen. 2013. Imaging energy status in live cells with a fluorescent biosensor of the intracellular ATP-to-ADP ratio. Nat Commun. 4: 1–25.
62. Tantama, M., and G. Yellen. 2014. Imaging changes in the cytosolic ATP-to-ADP ratio. Methods Enzym. 547: 355–371.

63. Civelek, V.N., J.T. Deeney, K. Kubik, V. Schultz, K. Tornheim, and B.E. Corkey. 1996. Temporal sequence of metabolic and ionic events in glucose-stimulated clonal pancreatic ß-cells (HIT). Biochem. J. 315: 1015–9.
64. Pathak, A., and S. Kumar. 2012. Independent regulation of tumor cell migration by matrix stiffness and confinement. Proc. Natl. Acad. Sci. 109: 10334–10339.
65. Amano, M., M. Nakayama, and K. Kaibuchi. 2010. Rho-kinase/ROCK: A key regulator of the cytoskeleton and cell polarity. Cytoskeleton. 67: 545–554.
66. Jekely, G., H.H. Sung, C.M. Luque, and P. Rorth. 2005. Regulators of endocytosis maintain localized receptor tyrosine kinase signaling in guided migration. Dev. Cell. 9: 197–207.
67. Shen, Q., R.R. Rigor, C.D. Pivetti, M.H. Wu, and S.Y. Yuan. 2010. Myosin light chain kinase in microvascular endothelial barrier function. Cardiovasc. Res. 87: 272–280.
68. Shen, L., and J.R. Turner. 2005. Actin Depolymerization Disrupts Tight Junctions via Caveolae-mediated Endocytosis. Mol. Biol. Cell. 16: 1–13.
69. Tantama, M., Y.P. Hung, and G. Yellen. 2011. Imaging Intracellular pH in Live Cells with a Genetically-Encoded Red Fluorescent Protein Sensor. J. Am. Chem. Soc. 133: 10034–10037.
70. McKenna, J.P., J. Ha, M.J. Merrins, L.S. Satin, A. Sherman, and R. Bertram. 2016. Ca2+ Effects on ATP Production and Consumption Have Key Regulatory Roles on Oscillatory Islet Activity. Biophys. J. (In Press): 733–742.
71. Carta, S., F. Penco, R. Lavieri, A. Martini, C.A. Dinarello, M. Gattorno, and A. Rubartelli. 2015. Cell stress increases ATP release in NLRP3 inflammasome-mediated autoinflammatory diseases, resulting in cytokine imbalance. Proc. Natl. Acad. Sci. U. S. A. 112: 2835–40.
72. Morris, B.A., B. Burkel, S.M. Ponik, J. Fan, J.S. Condeelis, J.A. Aguire-Ghiso, J. Castracane, J.M. Denu, and P.J. Keely. 2016. Collagen Matrix Density Drives the Metabolic Shift in Breast Cancer Cells. EBioMedicine. .
73. Egeblad, M., M.G. Rasch, and V.M. Weaver. 2010. Dynamic interplay between the collagen scaffold and tumor evolution. Curr. Opin. Cell Biol. 22: 697–706.
74. Langley, R.R., and I.J. Fidler. 2007. Tumor cell-organ microenvironment interactions in the pathogenesis of cancer metastasis. Endocr. Rev. 28: 297–321.
75. Levental, K.R., H. Yu, L. Kass, J.N. Lakins, J.T. Erler, S.F.T. Fong, K. Csiszar, A. Giaccia, M. Yamauchi, D.L. Gasser, and V.M. Weaver. 2009. Matrix Crosslinking Forces Tumor Progression by Enhancing Integrin signaling. Cell. 139: 891–906.
76. Pathak, A., and S. Kumar. 2011. Biophysical regulation of tumor cell invasion: moving beyond matrix stiffness. Integr. Biol. (Camb). 3: 267–278.
77. Baker, B.M., and C.S. Chen. 2012. Deconstructing the third dimension - how 3D culture microenvironments alter cellular cues. J. Cell Sci. 125: 3015–3024.
78. Nelson, C.M., and M.J. Bissell. 2010. Of Extracellular Matrix, Scaffolds, and Signaling: Tissue Architecture Regulates Development, Homeostasis, and Cancer. J. Phys. 22: 16–19.
79. Fraley, S.I., P.-H. Wu, L. He, Y. Feng, R. Krisnamurthy, G.D. Longmore, and

D. Wirtz. 2015. Three-dimensional matrix fiber alignment modulates cell migration and MT1-MMP utility by spatially and temporally directing protrusions. Sci. Rep. 5: 14580.
80. Provenzano, P.P., K.W. Eliceiri, J.M. Campbell, D.R. Inman, J.G. White, and P.J. Keely. 2006. Collagen reorganization at the tumor-stromal interface facilitates local invasion. BMC Med. 4: 38.
81. Riching, K.M., B.L. Cox, M.R. Salick, C. Pehlke, A.S. Riching, S.M. Ponik, B.R. Bass, W.C. Crone, Y. Jiang, A.M. Weaver, K.W. Eliceiri, and P.J. Keely. 2015. 3D collagen alignment limits protrusions to enhance breast cancer cell persistence. Biophys. J. 107: 2546–2558.
82. Baker, B.M., B. Trappmann, W.Y. Wang, M.S. Sakar, I.L. Kim, V.B. Shenoy, J.A. Burdick, and C.S. Chen. 2015. Cell-mediated fibre recruitment drives extracellular matrix matrix mechanosensing in engineered fibrillar microenvironments. Nat. Mater. 14.
83. Abhilash, A.S., B.M. Baker, B. Trappmann, C.S. Chen, and V.B. Shenoy. 2014. Remodeling of fibrous extracellular matrices by contractile cells: Predictions from discrete fiber network simulations. Biophys. J. 107: 1829–1840.
84. Guo, C.L., M. Ouyang, and J.Y. Yu. 2013. Long-range mechanical force enables self-assembly of epithelial tubules. Conf. Proc. Soc. Exp. Mech. Ser. 5: 15–21.
85. Lo, C.M., H.B. Wang, M. Dembo, and Y.L. Wang. 2000. Cell movement is guided by the rigidity of the substrate. Biophys. J. 79: 144–152.
86. Li, Q., Y. Zhang, P. Pluchon, J. Robens, K. Herr, M. Mercade, J.-P. Thiery, H. Yu, and V. Viasnoff. 2016. Extracellular matrix scaffolding guides lumen elongation by inducing anisotropic intercellular mechanical tension. Nat. Cell Biol. .
87. Ingber, D.E. 2009. Tensegrity-Based Mechanosensing from Macro to Micro Donald. Prog. Biophys. Mol. Biol. 97: 163–179.
88. Bershadsky, A.D., N.Q. Balaban, and B. Geiger. 2003. Adhesion-Dependent Cell Mechanosentivity. Annu. Rev. Immunol. 21: 305–334.
89. Friedl, P., and S. Alexander. 2011. Cancer invasion and the microenvironment: Plasticity and reciprocity. Cell. 147: 992–1009.
90. Lanfer, B., U. Freudenberg, R. Zimmermann, D. Stamov, V. K??rber, and C. Werner. 2008. Aligned fibrillar collagen matrices obtained by shear flow deposition. Biomaterials. 29: 3888–3895.
91. Liu, Z. 1991. Scale space approach to directional analysis of images. Appl. Opt. 30: 1369–1373.
92. Carey, S.P., A. Starchenko, A.L. McGregor, and C.A. Reinhart-King. 2014. Leading malignant cells initiate collective epithelial cell invasion in a three-dimensional heterotypic tumor spheroid model. Clin Exp Metastasis. 30: 615–630.
93. Maskarinec, S. a, C. Franck, D. a Tirrell, and G. Ravichandran. 2009. Quantifying cellular traction forces in three dimensions. Proc. Natl. Acad. Sci. U. S. A. 106: 22108–22113.
94. Franck, C., S.A. Maskarinec, D.A. Tirrell, and G. Ravichandran. 2011. Three-

dimensional traction force microscopy: A new tool for quantifying cell-matrix interactions. PLoS One. 6.
95. Jain, M. 2011. A next-generation approach to the characterization of a non-model plant transcriptome. Curr. Sci. 101: 1435–1439.
96. Pupa, S.M., S. Ménard, S. Forti, and E. Tagliabue. 2002. New insights into the role of extracellular matrix during tumor onset and progression. J. Cell. Physiol. 192: 259–267.
97. Angelica, M.D., and Y. Fong. 2008. Cell and tissue mechanics in cell migration. October. 141: 520–529.
98. Mundt, A.J., J.C. Roeske, T.D. Chung, and R.R. Weichselbaum. 2003. Holland-Frei Cancer Medicine. Hamilton (ON): BC Decker.
99. Gillie, J.K., J. Hochlowski, and G.A. Arbuckle-Keil. 2000. Infrared spectroscopy. Anal. Chem. 72: 71R–79R.
100. Li, J., D. Han, and Y.-P. Zhao. 2014. Kinetic behaviour of the cells touching substrate: the interfacial stiffness guides cell spreading. Sci. Rep. 4: 3910.
101. Xu, B., H. Li, and Y. Zhang. 2013. Understanding the viscoelastic behavior of collagen matrices through relaxation time distribution spectrum. Biomatter. 3: 1–8.
102. Chaudhuri, O., L. Gu, D. Klumpers, M. Darnell, S.A. Bencherif, J.C. Weaver, N. Huebsch, H.-P. Lee, E. Lippens, G.N. Duda, and D.J. Mooney. 2015. Hydrogels with tunable stress relaxation regulate stem cell fate and activity. Nat. Mater. 15: 326–334.
103. Siegel, R.L., K.D. Miller, and A. Jemal. 2015. Cancer statistics , 2015 . CA Cancer J Clin. 65: 21254.
104. 2014. SEER Cancer Statistics Review 1975-2011. Natl. Cancer Inst. : 1992–2011.
105. van Dongen, J.A., A.C. Voogd, I.S. Fentiman, C. Legrand, R.J. Sylvester, D. Tong, E. van der Schueren, P.A. Helle, K. van Zijl, and H. Bartelink. 2000. Long-term results of a randomized trial comparing breast-conserving therapy with mastectomy: European Organization for Research and Treatment of Cancer 10801 trial. J. Natl. Cancer Inst. 92: 1143–1150.
106. Gary.M. 2000. Local Recurrence After Mastectomy or Breast-Conserving Surgery and Radiation. J. Oncol. : 1–23.
107. Lê, M.G., R. Arriagada, M. Spielmann, J.-M. Guinebretière, and F. Rochard. 2002. Prognostic factors for death after an isolated local recurrence in patients with early-stage breast carcinoma. Cancer. 94: 2813–2820.
108. Bartelink, H. 2001. Recurrence Rates after treatment of breast cancer with Standard Radiotherapy With or Without Additional Radiation. NEJM. 345: 1378–1388.
109. Ozyigit, G., and M. Gultekin. 2014. Current role of modern radiotherapy techniques in the management of breast cancer. World J. Clin. Oncol. 5: 425–39.
110. Fisher, B., S. Anderson, C. Redmond, N. Wolmark, L. Wickerham, and W. Cronin. 1995. Reanalysis and results after 12 years of follow-up in a randomized clinical trial comparing total mastectomy with lumpectomy with or

without irradiation in the treatment of breast cancer b. N. Engl. J. Med. 333: 1456–1461.
111. Moncada S, H.A. 1993. Radiotherapy After Brest-Preserving Surgery in Women with Localized Cancer of the Breast. N Engl J Med. 329: 2002–2012.
112. Wickberg, A., L. Holmberg, H.-O. Adami, A. Magnuson, K. Villman, and G. Liljegren. 2014. Sector resection with or without postoperative radiotherapy for stage I breast cancer: 20-year results of a randomized trial. J. Clin. Oncol. 32: 791–7.
113. Tattini, C., J. Manchio, V. Zaporojan, G. Carderelli, L. Bonassar, A. Spangenberger, and J. Weinzweig. 2008. Role of TGF-β and FGF in the Treatment of Radiation-Impaired Wounds Using a Novel Drug Delivery System. Plast. Reconstr. Surg. 122: 1036–1045.
114. Ferguson, P.C., E.L. Boynton, J.S. Wunder, R.P. Hill, B. O'Sullivan, J.S. Sandhu, and R.S. Bell. 1999. Intradermal injection of autologous dermal fibroblasts improves wound healing in irradiated skin. J. Surg. Res. 85: 331–338.
115. Curran, D., J.P. Van Dongen, N.K. Aaronson, G. Kiebert, I.S. Fentiman, F. Mignolet, and H. Bartelink. 1998. Quality of life of early-stage breast cancer patients treated with radical mastectomy or breast-conserving procedures: Results of EORTC trial 10801. Eur. J. Cancer. 34: 307–314.
116. Di Lullo, G.A., S.M. Sweeney, J. Korkko, L. Ala-Kokko, and J.D. San Antonio. 2002. Mapping the Ligand-binding Sites and Disease-associated Mutations on the Most Abundant Protein in the Human, Type I Collagen. J. Biol. Chem. 277: 4223–4231.
117. Cinel, I., M. Ark, P. Dellinger, T. Karabacak, L. Tamer, L. Cinel, P. Michael, S. Hussein, J.E. Parrillo, and A. Kumar. 2012. Involvement of Rho kinase (ROCK) in sepsis - induced acute lung injury. J. Thorac. Dis. 4: 3–8.
118. Provenzano, P.P., D.R. Inman, K.W. Eliceiri, J.G. Knittel, L. Yan, C.T. Rueden, J.G. White, and P.J. Keely. 2008. Collagen density promotes mammary tumor initiation and progression. BMC Med. 6: 11.
119. Li, L.P., W. Herzog, R.K. Korhonen, and J.S. Jurvelin. 2005. The role of viscoelasticity of collagen fibers in articular cartilage: Axial tension versus compression. Med. Eng. Phys. 27: 51–57.
120. Bryan, M.A., J.W. Brauner, G. Anderle, C.R. Flach, and R. Mendelsohn. 2008. FTIR Studies of Collagen Model Peptides: Complementary Experimental and Simulation Approaches to Conformation and Unfolding. J. Am. Chem. Soc. 129: 7877–7884.
121. Vidal, B.D.C., and M.L.S. Mello. 2011. Collagen type I amide I band infrared spectroscopy. Micron. 42: 283–9.
122. Sheena Mary, Y., L. Ushakumari, B. Harikumar, H. Tresa Varhese, and C. Yohannan Panicker. 2009. FT-IR, FT-Raman and SERS Spectra of L-Proline. J. Iran. Chem. Soc. 6: 138–144.
123. Dietlein, F., L. Thelen, and H.C. Reinhardt. 2014. Cancer-specific defects in DNA repair pathways as targets for personalized therapeutic approaches. Trends Genet. 30: 326–339.

124. Stone, H.B., C.N. Coleman, M.S. Anscher, and W.H. McBride. 2003. Effects of radiation on normal tissue: Consequences and mechanisms. Lancet Oncol. 4: 529–536.
125. Forrest, a. P., H.J. Stewart, D. Everington, R.J. Prescott, C.S. McArdle, A.N. Harnett, D.C. Smith, and W.D. George. 1996. Randomized controlled trial of conservation therapy for breast cancer: 6-year analysis of the Scottish trial. Lancet. 348: 708–713.
126. Discher, D.E., P. Janmey, and Y.-L. Wang. 2005. Tissue cells feel and respond to the stiffness of their substrate. Science. 310: 1139–43.
127. Baker, E.L., J. Lu, D. Yu, R.T. Bonnecaze, and M.H. Zaman. 2010. Cancer Cell Stiffness: Integrated Roles of Three-Dimensional Matrix Stiffness and Transforming Potential. Biophys. J. 99: 2048–2057.
128. Chemie, B., and S. Louis. 2014. ECM stiffness paves the way for tumor cells. Int. Wound J. 11: 235–7.
129. Ross, G.M. 1999. Induction of cell death by radiotherapy. Endocr. Relat. Cancer. 6: 41–44.
130. Correia, A.L., and M.J. Bissell. 2012. The tumor microenvironment is a dominant force in multidrug resistance. Drug Resist. Updat. 15: 39–49.
131. Schrader, J., T.T. Gordon-Walker, R.L. Aucott, M. van Deemter, A. Quaas, S. Walsh, D. Benten, S.J. Forbes, R.G. Wells, and J.P. Iredale. 2011. Matrix stiffness modulates proliferation, chemotherapeutic response, and dormancy in hepatocellular carcinoma cells. Hepatology. 53: 1192–1205.
132. American Cancer Society. 2015. Cancer treatment & survivorship: Facts & Figures 2014-2015. .
133. Mogilner, A., and G. Oster. 1996. Cell motility driven by actin polymerization. Biophys. J. 71: 303–3045.
134. Ilić, D., Y. Furuta, S. Kanazawa, N. Takeda, K. Sobuet, N. Nakatsuji, S. Nomura, J. Fujimoto, J. Fujimoto, T. Yamamoto, and S. Aizawa. 1995. Reduced cell motility and enhanced focal adhesion contact formation in cells from FAK-deficient mice. Nature. 377: 539–544.
135. Abercrombie, M., J.E. Heaysman, and S.M. Pegrum. 1970. The locomotion of fibroblasts in culture. I. Movements of the leading edge. Exp. Cell Res. 59: 393–398.
136. Petrie, R.J., N. Gavara, R.S. Chadwick, and K.M. Yamada. 2012. Nonpolarized signaling reveals two distinct modes of 3D cell migration. J. Cell Biol. 197: 439–455.
137. Friedl, P., and K. Wolf. 2010. Plasticity of cell migration: A multiscale tuning model. J. Cell Biol. 188: 11–19.
138. Doyle, A.D., F.W. Wang, K. Matsumoto, and K.M. Yamada. 2009. One-dimensional topography underlies three-dimensional fi brillar cell migration. J. Cell Biol. 184: 481–490.
139. Sanz-Moreno, V., and C.J. Marshall. 2010. The plasticity of cytoskeletal dynamics underlying neoplastic cell migration. Curr. Opin. Cell Biol. 22: 690–696.
140. Friedl, P., and K. Wolf. 2003. Tumour-cell invasion and migration: Diversity

and escape mechanisms. Nat. Rev. Cancer. 3: 362–374.
141. Doyle, A.D., R.J. Petrie, M.L. Kutys, and K.M. Yamada. 2013. Dimensions in Cell Migration. Curr. Opin. Cell Biol. 25: 642–649.
142. Gerecht, S., C.J. Bettinger, Z. Zhang, J. Borenstein, G. Vunjak-Novakovic, and R. Langer. 2007. The effect of actin disrupting agents on contact guidance of human embryonic stem cells. Biomaterials. 28: 4068–4077.
143. Yeung, T., P.C. Georges, L.A. Flanagan, B. Marg, M. Ortiz, M. Funaki, N. Zahir, W. Ming, V. Weaver, and P.A. Janmey. 2005. Effects of substrate stiffness on cell morphology, cytoskeletal structure, and adhesion. Cell Motil. Cytoskeleton. 60: 24–34.
144. Boudreau, N., C.J. Sympson, Z. Werb, and M.J. Bissell. 1995. Suppression of ICE and Apoptosis in Mammary Epithelial Cells by Extracellular Matrix. Science (80-.). 267: 891–893.
145. Gospodarowicz, D., D. Delgado, and I. Vlodavsky. 1980. Permissive effect of the extracellular matrix on cell proliferation in vitro. Proc. Natl. Acad. Sci. U. S. A. 77: 4094–4098.
146. Lin, C.Q., and M.J. Bissell. 1993. Multi-faceted regulation of cell differentiation by extracellular matrix. FASEB J. 7: 737–743.
147. Stetler-Stevenson, W.G., S. Aznavoorian, and L.A. Liotta. 1993. TUMOR CELL INTERACTIONS WITH THE EXTRACELLULAR MATRIX DURING INVASION AND METASTASIS. Annu. Rev. Cell. Biol. 9: 541–573.
148. Lutolf, M.P., and J.A. Hubbell. 2005. Synthetic biomaterials as instructive extracellular microenvironments for morphogenesis in tissue engineering. Nat. Biotechnol. 23: 47–55.
149. Cross, V.L., Y. Zheng, N.W. Choi, S.S. Verbridge, A. Bryan, L.J. Bonassar, C. Fischbach, and A.D. Stroock. 2011. Dense type I collagen matrices that support cellular remodeling and microfabrication for studies of tumor angiogenesis and vasculogenesis in vitro. Biomaterials. 31: 8596–8607.
150. Ghajar, C.M., K.S. Blevins, C.C.W. Hughes, S.C. George, and A.J. Putnam. 2006. Mesenchymal Stem Cells Enhance Angiogenesis in Mechanically Viable Prevascularized Tissues via Early Matrix Metalloproteinase Upregulation. Tissue Eng. 0: 060928131519005.
151. Seidlits, S.K., C.T. Drinnan, R.R. Petersen, J.B. Shear, L.J. Suggs, and C.E. Schmidt. 2011. Fibronectin-hyaluronic acid composite hydrogels for three-dimensional endothelial cell culture. Acta Biomater. 7: 2401–2409.
152. Swartz, M.A., D.J. Tschumperlin, R.D. Kamm, and J.M. Drazen. 2001. Mechanical stress is communicated between different cell types to elicit matrix remodeling. Proc. Natl. Acad. Sci. U. S. A. 98: 6180–6185.
153. Mason, B.N., A. Starchenko, R.M. Williams, L.J. Bonassar, and C. a. Reinhart-King. 2013. Tuning three-dimensional collagen matrix stiffness independently of collagen concentration modulates endothelial cell behavior. Acta Biomater. 9: 4635–4644.
154. Ehrbar, M., A. Sala, P. Lienemann, A. Ranga, K. Mosiewicz, A. Bittermann, S.C. Rizzi, F.E. Weber, and M.P. Lutolf. 2011. Elucidating the role of matrix

stiffness in 3D cell migration and remodeling. Biophys. J. 100: 284–293.
155. Kraehenbuehl, T.P., P. Zammaretti, A.J. Van der Vlies, R.G. Schoenmakers, M.P. Lutolf, M.E. Jaconi, and J.A. Hubbell. 2008. Three-dimensional extracellular matrix-directed cardioprogenitor differentiation: Systematic modulation of a synthetic cell-responsive PEG-hydrogel. Biomaterials. 29: 2757–2766.
156. Kloxin, A.M., A.M. Kasko, C.N. Salinas, and K.S. Anseth. 2009. Photodegradable hydrogels for dynamic tuning of physical and chemical properties. Science (80-.). 324: 59–63.
157. Zhang, G., C.T. Drinnan, L.R. Geuss, and L.J. Suggs. 2010. Vascular differentiation of bone marrow stem cells is directed by a tunable three-dimensional matrix. Acta Biomater. 6: 3395–3403.
158. Ramasamy, R., S.F. Yan, and A.M. Schmidt. 2012. Advanced glycation endproducts: from precursors to RAGE: round and round we go. Amino Acids. 42: 1151–1161.
159. Li, D., and Y. Xia. 2004. Electrospinning of nanofibers: Reinventing the wheel? Adv. Mater. 16: 1151–1170.
160. Guo, C., and L.J. Kaufman. 2007. Flow and magnetic field induced collagen alignment. Biomaterials. 28: 1105–1114.
161. Tian, Z., K. Wu, W. Liu, L. Shen, and G. Li. 2015. Two-dimensional infrared spectroscopic study on the thermally induced structural changes of glutaraldehyde-crosslinked collagen. Spectrochim. Acta - Part A Mol. Biomol. Spectrosc. 140: 356–363.
162. Tian, H., Y. Chen, C. Ding, and G. Li. 2012. Interaction study in homogeneous collagen/chondroitin sulfate blends by two-dimensional infrared spectroscopy. Carboyhydrate Polym. 89: 542–550.
163. Bordeleau, F., J.P. Califano, Y.L. Negrón Abril, B.N. Mason, D.J. LaValley, S.J. Shin, R.S. Weiss, and C.A. Reinhart-King. 2015. Tissue stiffness regulates serine/arginine-rich protein-mediated splicing of the extra domain B-fibronectin isoform in tumors. Proc. Natl. Acad. Sci. 112: 8314–8319.

PART II

STAND-OFF PULSE POWER PLASMA FUSION

Joseph Patrick Miller
2018

A typical plasma pinch system involves passing a current of 10^5-10^7 amperes in approximately 10^{-7} seconds thru thin filaments, 4-25um in diameter. This pulse generates a strong magnetic field resulting in a contracting Lorentz force that increases the filament temperature and pressure. This increased temperature causes the formation of a plasma and x-ray production. It has been theorized these x-rays can be used to compress a fusion fuel pellet to the point of meeting the Lawrence conditions for sustained energy production. In order to create such intense currents, some mechanism to generate significant pulsed-power must be adopted. However, there are considerable complications regarding the capacitor banks capable of delivering current in this range. Specifically, they are very expensive, occupy large areas and must be directly attached to the filament assembly. This direct contact complicates the effort considerably by introducing the so-called "*Kopek Problem",* which is the requirement of having to replace constructive material destroyed by temperature and irradiative stresses between shots. Currently, Sandia National Labs' *Z-Machine* produces the world's largest electrical discharge on the order of 10^7 amperes. *Z* utilizes a capacitor bank that occupies the size of a gymnasium and cost more than $80 million dollars to construct. At another scale, Cornell University operates two pulsed-power machines: COBRA and XP Pulser, which deliver approximately 0.9-1.2MA in 95-235ns rise time and 500kA in 50ns rise time, respectively; both of which are powered by

capacitor banks wired directly to the filament arrangements. What is needed for future fusion research is an inexpensive, standoff mechanism to generate the necessary pulses for fusion systems and more generally, plasma research.

Pulsed-power systems operate under simple principles. The system stores electrical energy (Q) over a long period of time and delivers it over a much shorter period of time ($t_{delivery}$) with some efficiency (η). Thus, the total power delivered is simply $P = Q\eta/t_{delivery}$. Clearly, to produce a large pulse of power, the best systems will store large amounts of charge and deliver it over a very short period of time. To this end, we have built a simple cantilever system capable of being remotely charged via an electron beam to a mechanically tunable voltage and discharged in the nanosecond regime. This design allows for large Q and circumvents the Kopek Problem by remote charging. The cantilever functions by acquiring charge from the electron beam until the *pull-in voltage* is achieved and the cantilever abruptly shuts, allowing current to flow. Since the cantilever's pull-in voltage is purely a function of physical parameters and the rise time can be on the order of nanoseconds, it is feasible a cantilever-based device can be designed such that the required current for plasma formation can be achieved and indeed, even the potential for ignition in fiber-pinch fusion operations. Presented here are the design and results of experiments carried out on a copper cantilever system between the charging electron-beam energies of 1keV to 10keV.

Chapter 6

Cantilever-Based Current Pulse

6.1 Theory

An electrostatically actuated cantilever experiences two primary forces in vacuum. The first is a restoring spring force and the second is the electrostatic attraction between the cantilever and the ground plane. The applied voltage necessary for the electrostatic force to overwhelm the spring force is called the *pull-in voltage*. This voltage is entirely a function of physical variables such as the dimensions of the cantilever, the modulus, the distance between the plates, and the dielectric permittivity between them. To turn the cantilever system into a pulsed-power system, the cantilever is designed to have a pull-in voltage that will provide a pulse appropriate for the application. As mentioned, power delivery is given by $P = Q\eta/t_{delivery}$, where $t_{delivery}$ is approximated as 10^{-9}s. Thus, the cantilever is designed to control the total charge stored, Q, before pull-in is achieved. The amount of charge stored on a generic capacitor is equal to the capacitance (C) times the voltage (V).

$$Q = CV \tag{1}$$

Where the capacitance C of an electrostatic actuator, such as a cantilever, is given by:

$$C = \varepsilon \frac{A}{g} \tag{2}$$

In (eq.2), g is the gap or distance between the cantilever and the bottom electrode; A is the area of the projected overlap between the two electrodes. This implies that the

maximum current (*dQ/dt*) from the discharge at the pull-in voltage (V_{max}) has the relationship:

$$_{max} = \frac{\varepsilon A}{gt} V_{max} \tag{3}$$

What remains to understand are the variables involved in V_{max}. In the parallel plate approximation of a cantilever, this voltage can be derived from the total potential energy in the system:

$$U = -\frac{\varepsilon A}{2(g-x)} V^2 + \frac{kx^2}{2} \tag{4}$$

Where the first term is the potential from the capacitor, *x* is the displacement of the cantilever from rest and the second term is from the energy in the restoring spring force. Taking the derivative, we get the force acting on the cantilever:

$$F = -\frac{dU}{dx} = -\frac{\varepsilon A}{2(g-x)^2} V^2 - kx \tag{5}$$

The equilibrium condition implies:

$$kx = \frac{\varepsilon A}{2(g-x)^2} V^2 \tag{6}$$

At this point, the restoring spring force of the cantilever is in balance with the electrostatic attraction of the cantilever with the ground plane. The voltage that meets this condition is directly proportional to the maximum amount of charge the cantilever can store before instability (eq.1). Because the cantilever is designed around this equilibrium point, the relationship for the cantilever position as a function of the voltage must be derived. To do so, one first solves for the change in the force for a change in the position:

$$\frac{dF}{dx} = \frac{\varepsilon A}{(g-x)^3} V^2 - k \tag{7}$$

Applying the equilibrium condition from equation (eq.6), the first term yields the "stiffness" around the equilibrium point:

$$\frac{dF}{dx} = \frac{2kx}{(g-x)} - kx \tag{8}$$

From (eq.7), one can see that when no electrostatic force is present (eq.7) reduces to Hooke's law; a small displacement generates a *negative* force to *decrease* x. Increasing the voltage will equilibrate the positive electrostatic force with the negative spring force ($dF/dx = 0$) and x can be solved to be 1/3rd of g. This is the stable point in the pull-down dynamics of the cantilever. However, if the voltage is further increased, x grows beyond this equilibrium point and the stiffness becomes *positive* and *increases* x. This effect is known as pull-in instability. An expression for the voltage on the cantilever at this point can be found by substituting the stability condition ($x=g/3$) into the equilibrium (eq.6).

$$V_{PI} = \sqrt{\frac{8}{27}\frac{kg^3}{\varepsilon A}} \tag{9}$$

(eq.9) makes it clear that the maximum charge a cantilever pulse-power system can store is dependent only on physical parameters. Finally, one can obtain an expression for maximum current by substituting (eq.9) into (eq.3).

$$I_{max} = 0.544 \cdot \frac{\sqrt{\varepsilon A k g}}{t} \tag{10}$$

Likewise, the numerator of (eq.10) is composed entirely of variables in the design space of the cantilever. The relative permittivity, ε may be modified by changing the dielectric between the cantilever and the ground electrode. Obviously the area of the cantilever is tunable as well as the gap, which now represents the maximum charge

accumulated on the cantilever. Finally, the spring constant, *k*, is a function of the material properties and physical dimensions. If one rewrites *k* in terms of its fundamental units, the following equation is produced:

$$I_{max} = 0.272 \cdot \frac{w\sqrt{Y\varepsilon g h^3}}{lt} \tag{11}$$

Where the dimensions *w,l,h* are the width, length, and height (thickness) of the cantilever, respectively. *Y* is the Young's modulus of the cantilever. Since plasma-pinch operation requires a current of 10^5-10^6 amperes, one only needs to determine the dimensions necessary to achieve this according to (eq.11) for a given material. As a proof of principle, a cantilever made of copper (*Young's Modulus = 120GPa*) with dimensions: 8.7mm x 67.1mm x 100um, at a 1cm gap from the bottom electrode has a theoretical current limit of I_{max} = 727mA (Figure 6.1) if it can achieve a pulse rise time of 5ns. The following describes the results of experiments conducted with such a cantilever pulse-power system.

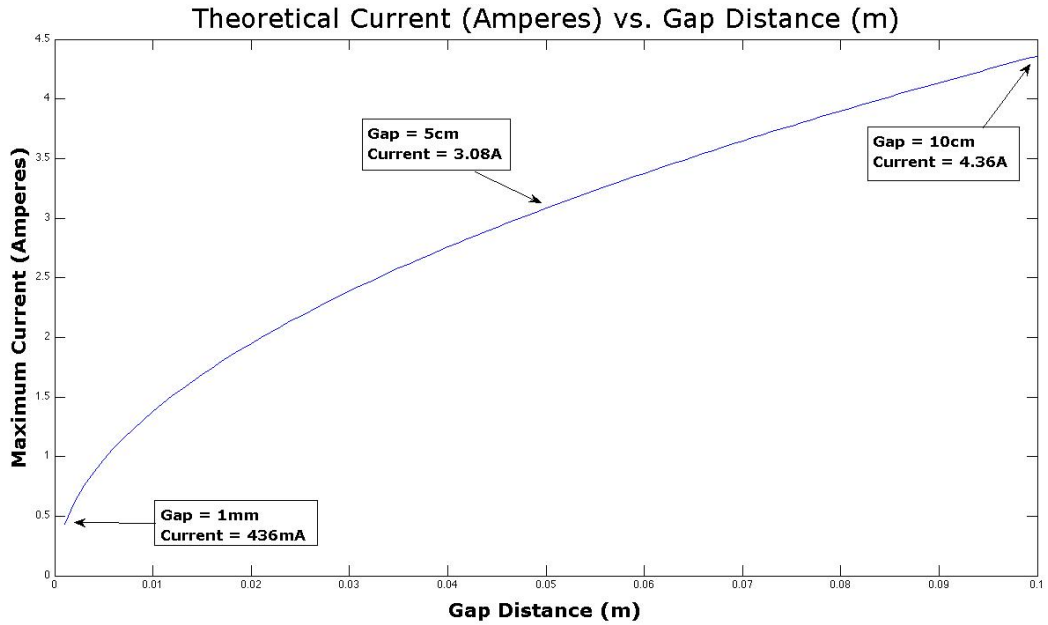

Figure 6.1. Theoretical current curve for 8.7mm x 67.1mm x 100um copper cantilever with a rise time of 5ns at various gap distances / pull-in voltages.

6.2 Pull-In Voltage

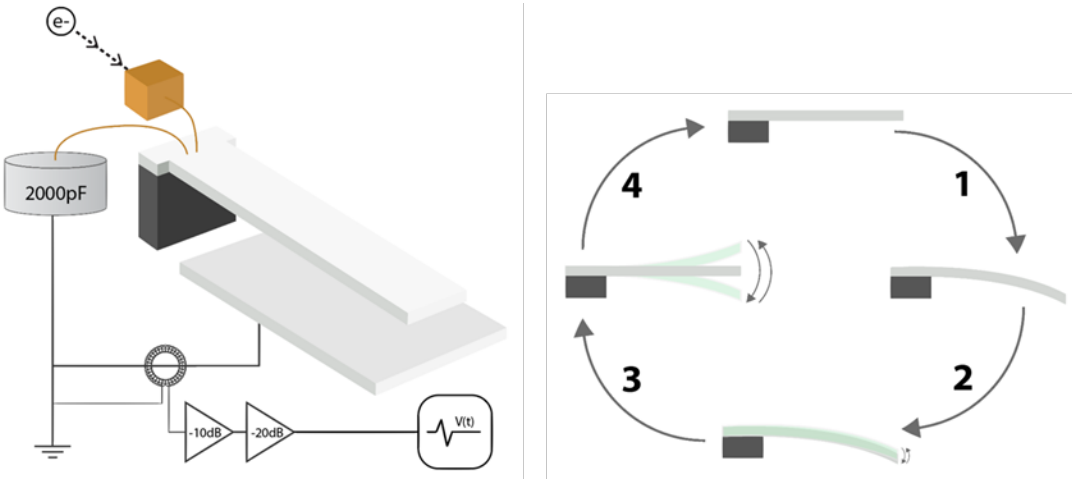

Figure 6.2. (Left) The operating principle - an electron beam is collected by the Faraday cup connected to a cantilever with a 200pF storage capacitor. The drain electrode collects the charge once the cantilever undergoes motion under pull-in instability. The current in the drain is measured by a Rogowski coil, which measures the current using Faraday's law due to the induced electric field in the coil due to the magnetic flux generated by the current. (Right) Cantilever bends under charging (1) and discharges (2) after pull-in. After the cantilever is drained, the cantilever mechanically oscillates for a few cycles as it loses energy (3) and starts charging again (1).

Electron guns can produce electrons of energies from kilovolts to megavolts.

Cantilevers with corresponding high pull-in voltages can also be designed. A copper cantilever with length l_C, width $w = l_C/10$, thickness $t = l_C/50$ has a pull-in voltage that can be written as (in Volts):

$$V_{PI} = 8.96 \cdot 10^7 \cdot \sqrt{\frac{g_0}{l_C}} \tag{12}$$

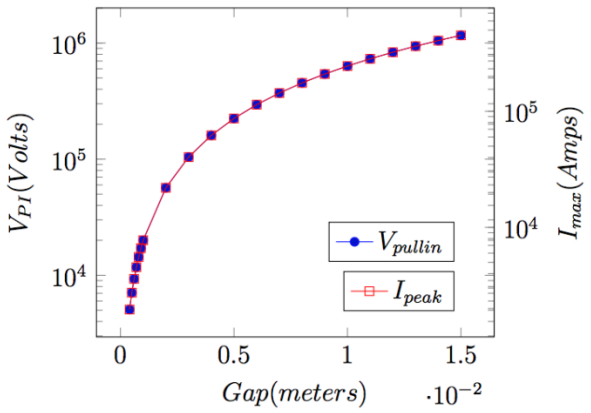

Figure 6.3. The Pull-In Voltage and Maximum Current by electrode gap.

6.3 Oscillation Dynamics

As the cantilever accumulates charge and pull-in is achieved, the instability causes the cantilever to have such momentum that upon impact, the reversal of the momentum occurs at a rate such that complete discharge has insufficient time to occur. As a result of this left over charge and the constant re-charging from the accelerator source, the cantilever has not fully reset and the subsequent discharge happens more rapidly than the initial pull-in. The resulting behavior is a rapid oscillation of discharges until the spring force of the cantilever overwhelms the electric force to reset the cycle completely.

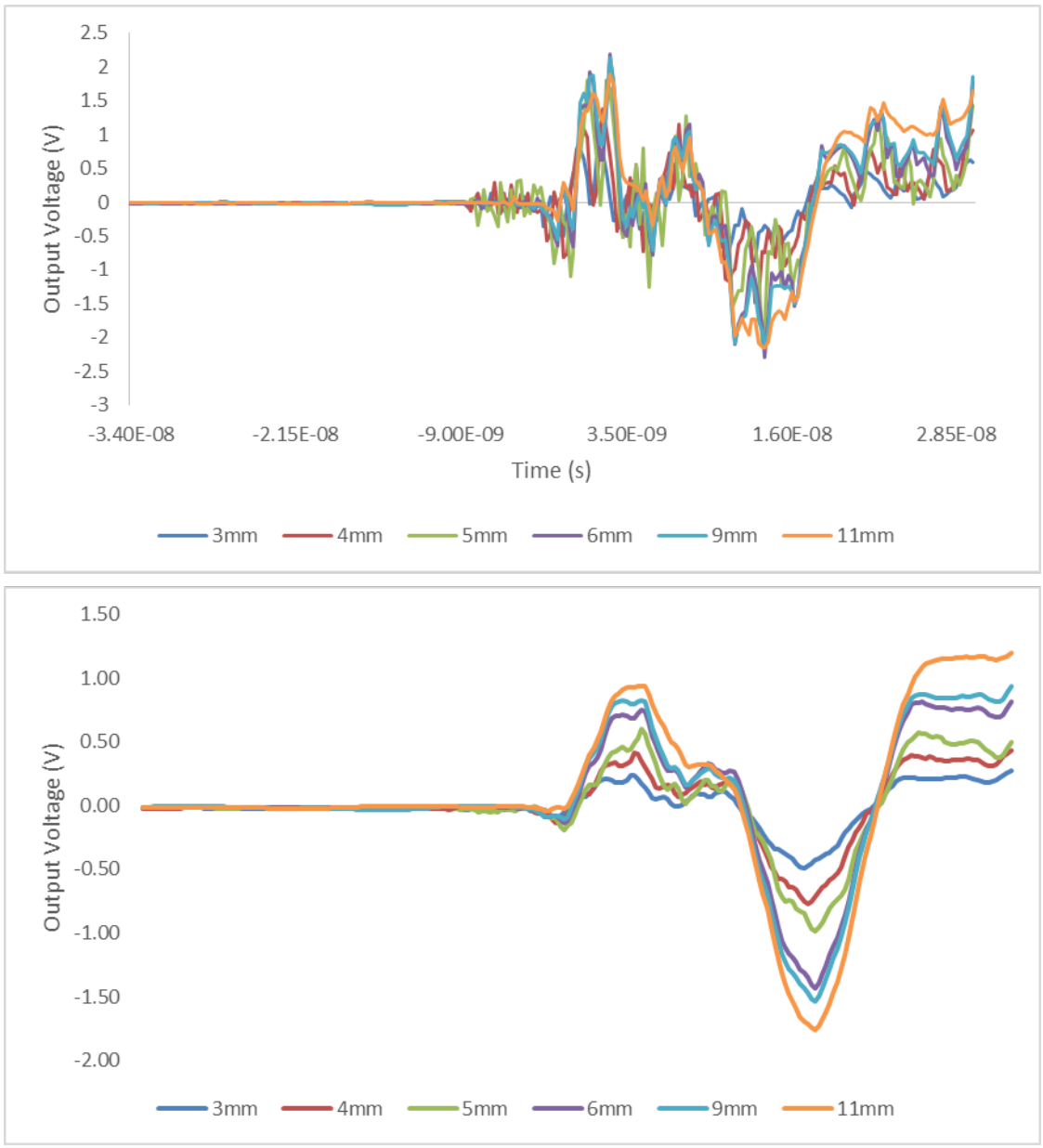

Figure 6.4. (Top) Oscillation of output voltage. (Bottom) Smoothed 5ns moving average.

6.4 Peak Current

The wire carrying currents is driven through the center of a Rogowski coil, which is used to measure the current amplitude. Parameters for the Rogowski Coil are listed in Table 1. The magnetic field generated from the current *i* induces a voltage in the coil

V_{coil} = M(di/dt), where M is the mutual inductance between the current carrying wire and the Rogowski coil. The output of the coil RC is loaded into an attenuator with a 50 Ω impedance. The device setup is defined in the following tables:

Table 6.1. Parameters of the cantilever

Cantilever length	l_C	70.00mm
Cantilever thickness	t_C	0.10mm
Cantilever width	w_C	15.00mm
Copper resistivity	ρ	1.8×10^{-7}
Cantilever inductance	$L_S = \frac{\mu_0}{2\pi} l_C (ln(\frac{2l_C}{w_C + t_C}) + 0.5 + 0.223 \frac{t_C + w_C}{l_c})$	38.8nH
Cantilever resistance	$R_S = \frac{\rho l_C}{t_C w_C}$	0.0084 Ω
Inductance impedance	$\lvert\omega_{res} L_S\rvert$	1.68Ω
Inductance impedance vs. Resistance	$\lvert\omega_{res} L_S\rvert / R$	200

Table 6.2. Parameters of the connection wires

Wire Length	l_{wire}	19cm
Wire radius	r_{wire}	0.5 mm
Wire inductance	$L_{wire} = \frac{\mu_0 l_{wire}}{2\pi} (\frac{ln(2l_{wire})}{r_{wire}} - 0.75)$	$223.68nH$
Wire resistance	$R_{wire} = \frac{\rho l_{wire}}{\pi r_{wire}^2}$	0.044Ω

Table 6.3. Rogowski coil parameters

Coil inner diameter	a	10.03 mm
Coil outer diameter	b	13.85 mm
Coil width	$d_{rc} = b - a$	3.82 mm
Coil wire thickness	d	6.00 mm
Number of turns	N	20
Mutual Inductance	$M = \frac{\mu_0 N}{2} (\sqrt{\frac{b}{2}} - \sqrt{\frac{a}{2}})^2$	$1.93nH$
Calibrated Mutual Inductance	M_c	$5.31nH$
Coil Inductance	$L_{RC} = \frac{\mu_0 N^2 d_{rc}}{2\pi} ln(\frac{b}{a})$	$98.6nH$
Coil Capacitance	$C_{RC} = \frac{4\pi^2 \epsilon_0 (b+a)}{ln(\frac{b+a}{b-a})}$	$4.55pF$
Coil Resistance	$R_{RC} = \rho_c \frac{l_w}{\pi d^2}$	0.042Ω

The results of the cantilever pull in were measured as described and captured by high speed camera. Measured peak current, accounting for contact resistance was found to be in agreement with theoretical expectations as a function of electron beam energy

(Figure 6.5). In addition, the high speed camera was able to capture plume formation, however at the resolution of a single frame (Figure 6.6).

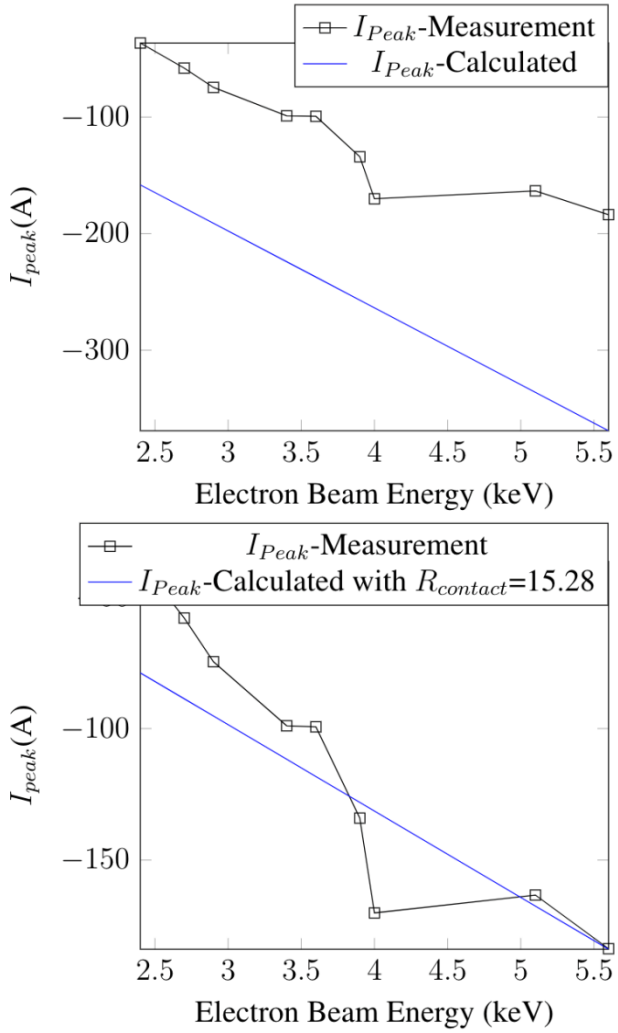

Figure 6.5. Peak current outputs relative to theoretical calculations.

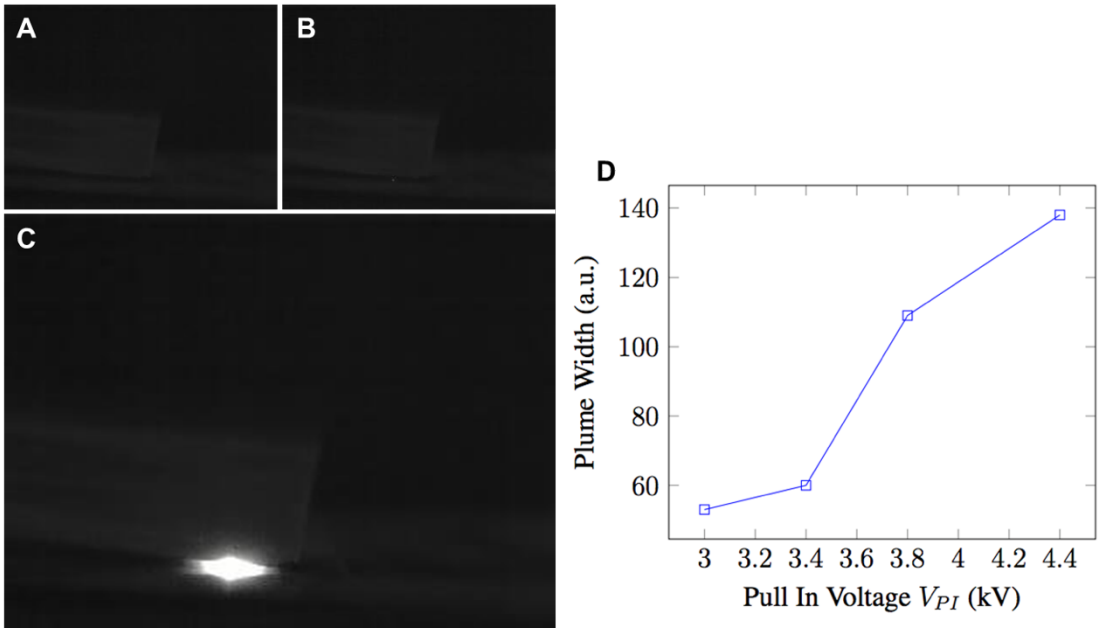

Figure 6.6. (A-C) High-Speed Camera Footage of Pull-In Pulse Event. (D) Ellipse fitted major-axis width by Pull-In voltage.

6.1 Conclusion and Future Work

Cantilever dynamics that exploit the pull-in voltage instability are common in the field of MEMS, typically for the useful application as sensitive switches. Very little research has been applied to the potential of large pull-in voltage requirements and how they might be used as a pulse-power mechanism. The results here are the first demonstrated Beam Charged Electrostatic Pulldown Pulser (BCEPP). This simple copper device has surprising complexity, however predictable behavior. The scaling of such a device to the necessary conditions for fusion suggest an entirely novel approach to pulse-plasma fiber punch fusion. The analysis of the peak current pulses is in agreement with the theory, although more careful experimental controls are needed to measure the peak currents, and the parasitics controlling the discharges. The scaling analysis predicts that Mega-Amperes of currents can be generated using the

cantilevers by scaling the current or the electron energy and pull-in voltage of the cantilevers. This initial method points to a future of possibility to achieve non-linear plasma phenomenon at very high current levels with a simple, low-cost, structure that can be placed in the path of high energy electron beams.

APPENDIX I

Cell Culture and Reagents

Metastatic MDA-MB-231 breast adenocarcinoma cells (HTB-26; ATCC, Rockville, MD) were maintained in Dulbecco's Modified Eagle's Medium (DMEM; Life Technologies, Grand Island, NY), supplemented with 10% fetal bovine serum (FBS; Atlanta Biologicals, Flowery Branch, GA) and 1% penicillin-streptomycin (Life Technologies). HEK293T cells were a gift from Dr. Michael King (Cornell University, Ithaca, NY, USA) and were cultured in Minimum Essential Medium supplemented with 10% fetal bovine serum and 1% penicillin-streptomycin (Invitrogen). All cells were cultured at 37 °C and 5% CO_2. All cell culture, fluorescent imaging, and time-lapse imaging were performed at 37°C and 5% CO_2.

DNA constructs and lentiviral transductions

FUGW-PercevalHR (Addgene plasmid # 49083) and GW1-pHRed (Addgene plasmid # 31473) were gifts from Dr. Gary Yellen (Harvard Medical School, Boston, MA, USA). The lentiviral vector pFUW-CMV and pSPAX2 and pMD2G plasmids were gifts from Dr. Michael King (Cornell University, Ithaca, NY, USA). The pHRed sensor was inserted into the pFUW-CMV vector using BamH1 and EcoR1 restriction sites to generate pFUW-CMV-pHRed. PercevalHR and pHRed lentiviral particles were prepared by transient transfection of HEK293T cells with the lentiviral expression vectors and the second generation packing constructs pSPAX2 and pMD2G in the presence of TransIT-LT1 (Mirus). Lentiviral particles were harvested from the HEK293T supernatant at 48 and 72 hours post-transfection and concentrated

100-fold with Lenti-X Concentrator (Clontech) followed by stable MDA-MB-231 cell transduction in the presence of 8 μg/mL polybrene overnight (Santa Cruz Biotechnology).

Cell Seeding in 2D and 3D

In 2D studies, cells were seeded in 96 well MatTek glass bottom dishes at 16,000cells/cm^2. Cells were overlaid with culture medium and allowed to adhere and spread overnight in a temperature-, humidity-, and CO_2-controlled incubator.

In 3D studies, cells were seeded at 125,000cells/mL in 3D collagen matrices prepared from acid-solubilized type I rat tail tendon collagen as previously described [8, 10]. 1.5mg/mL collagen solutions were made from a 10mg/mL collagen stock solution, diluted with cooled DMEM complete media and neutralized with 1N NaOH. Collagen matrices were allowed to polymerize at 37°C for 30min before being overlaid with culture medium.

For inhibitor studies, the following were used: ROCK inhibitor Y27632, PI3 kinase inhibitor LY294002 (20 μM; EMD Millipore, Billerica, MA), MLC kinase *inhibitor ML7, and* actin cytoskeleton inhibitor Latrunculin A (LatA). The media in each well was replaced with fresh DMEM Complete Media consisting of each inhibitor at the concentration indicated. The treated cells were incubated for 1hr at 37°C before being imaged.

Matrix Alignment

Collagen matrix was aligned by pulling paramagnetic polystyrene beads (PM-20-10; Spherotech, Lake Forest, IL) through the collagen during matrix polymerization using a magnetic field (160). Metal beads were combined with the cell/collagen solution at 1% (v/v). This solution was added to one well of a custom cell culture device comprising polydimethylsiloxane (PDMS) walls attached to a No. 1 coverglass. The other well was filled with the same solution without metal beads as a comparable random matrix control. The custom device was placed next to a neodymium magnet (BZX0Y0X0-N52; K&J Magnetics, Pipersville, PA) with surface field strength > 4kG to induce the magnetic field on the metal beads. Matrices were allowed to polymerize for 30min at room temperature before being overlaid with culture medium and imaged.

Confocal and Phase Contrast Imaging

Confocal fluorescence imaging of cells on glass and in 3D matrices was obtained on a Zeiss LSM700 confocal microscope using a 40x long working distance water immersion objective. Images were acquired after cells were cultured overnight. All time-lapse phase contrast imaging was performed on a Zeiss Axio Observer Z1 inverted microscope equipped with a Hamamatsu ORCA-ER camera. Images were collected >200μm above the bottom surface of 3D matrices at 20min intervals using a 10x objective over 24hrs.

ATP/ADP Ratios & Cell Migration Analysis from Time-Lapse Imaging

All image analysis was performed using ImageJ. The background noise from ATP and ADP images was removed to minimize interference by mean subtraction. The whole cell's fluorescence intensity was measured to acquire the ATP and ADP levels for a cell. The ATP level was divided by its respective ADP level to obtain the ATP/ADP ratio for a cell. As the microenvironment can affect intracellular pH, which in turn affects the intensity observed by the PercevalHR sensor, ATP/ADP ratios were normalized to a pHred sensor to correct for pH differences. This was done imaging with the RFP-based pHRed sensor as described previously (69).

For migration studies, cells were analyzed between 12-18hrs after seeding. Step-wise velocities were calculated by tracking the cells' centroids over time.

PDMS Molds & Alignment

PDMS molds (Sylgard 184 Elastomer Kit) were created with silicone elastomer base manually mixed with the silicone elastomer curing agent (10:1 by weight) for 10 min. The mixture was then de-gassed in a vacuum chamber for 5 h before being poured into a Falcon 150 mm x 15 mm petri dish and left to polymerize for 12 h at 60^0C. Molds were cut 3 cm x 1.5 cm with a 0.25 cm x 2.25 cm cavity. Molds were 0.5 cm thick. Molds were then 'activated', in order to secure collagen to the inner walls, by being placed in a Harrick Plasma PDL-001 Plasma Cleaner on high RF power for 2 min, submerged in 1% poly(ethyleneimine) solution (Fluka Analytical; Lot # MKBR5743V) in Milli-Q water for 5 min, washed twice (5 min/wash) with Milli-Q water, submerged in 0.01% glutaraldehyde solution (Sigma-Aldrich; Lot #

SLBJ4639V) in PBS (1x; non-sterile) for 30 min, and washed twice more with Milli-Q water.

Collagen Preparation

Collagen was harvested from Sprague-Dawley rat tail tendons as previously described(18, 22). Briefly, tendon bundles were removed and suspended in a 0.1% acetic acid solution at 150 mL/g tendon. The mixture was allowed to sit at 4°C for at least 48 h and then centrifuged at 9000 RPM for 90 min. The supernatant was collected, frozen and lyophilized for 48 h or until all water was removed. Stock solutions containing the lyophilized collagen reconstituted in acetic acid were prepared at 6 mg/mL and stored at 4°C until use. Working solutions containing 10x Dulbecco's Phosphate Buffered Saline (PBS), 1 N NaOH and 1x Dulbecco's Modified Eagles Medium (DMEM) were prepared and mixed with stock solutions, resulting in gels at 2.5 and 5 mg/mL collagen density. Each gel was then allowed to polymerize at 37°C for 30 min.

Single Cell and Tumor Spheroid Encapsulation

Tumor spheroids were prepared using methods adapted from previous work(92). Briefly, a mixture containing a suspension of MDA-MB-231 cells in DMEM/F12 (1:1) (Life Technologies) supplemented with 0.25% methocult (STEMCELL Technologies, Vancouver, BC), 5% horse serum (Life Technologies), 20 ng/mL hEGF (Life Technologies), 0.5 mg/mL hydrocortisone (Sigma Aldrich, St. Louis, MO), 100

ng/mL cholera toxin (Sigma Aldrich), 10 μg/mL insulin (Sigma Aldrich), 100 μg/mL penicillin and 100 g/mL streptomycin (Life Technologies). The mixture was pipetted into a round bottom 96-well plate such that each well contained 5,000 cells in 200 μL of media/0.25% methocult mixture. The plate was centrifuged at 1100 RPM for 5 min at room temperature and then incubated for 3 days at 37°C and 5% CO_2. After 3 days, cells compacted to form spheroids, which were removed from the 96-well plate and embedded in cantilevers containing 2.5 mg/mL type I collagen gels. Only spheroids embedded at least 200 μm above the bottom of the cantilever and at least 200 μm away from the cantilever wall were included in the study.

ATP/ADP Lentiviral Transductions

MDA-MB-231 cells with lentiviral transductions were prepared and visualized as described previously(61). Briefly, FUGW-PercevalHR (Addgene plasmid # 49083) and GW1-pHRed (Addgene plasmid # 31473) were gifts from Dr. Gary Yellen (Harvard Medical School, Boston, MA, USA). The lentiviral vector pFUW-CMV and pSPAX2 and pMD2G plasmids were gifts from Dr. Michael King (Cornell University, Ithaca, NY, USA). The pHRed sensor was inserted into the pFUW-CMV vector using BamH1 and EcoR1 restriction sites to generate pFUW-CMV-pHRed. PercevalHR and pHRed lentiviral particles were prepared by transient transfection of HEK293T cells with the lentiviral expression vectors and the second generation packing constructs pSPAX2 and pMD2G in the presence of TransIT-LT1 (Mirus). Lentiviral particles were harvested from the HEK293T supernatant at 48 and 72 h post-transfection and concentrated 100-fold with Lenti-X Concentrator (Clontech) followed by stable MDA-

MB-231 cell transduction in the presence of 8 μg/mL polybrene overnight (Santa Cruz Biotechnology). Cells were imaged using confocal microscopy and analyzed as previously described(61, 69).

Immunofluorescent Staining

Samples were fixed in 3.2% paraformaldehyde (PFA) for 15 min at room temperature, followed by three washes with 1x PBS. Cells were then permeabilized in 1% Triton X-100 for 1 h at room temperature, followed by three washes in 0.02% Tween 20 for 15 min each. Samples were incubated in Texas Red-X Phalloidin (1:50 dilution; Molecular Probes, T7471) overnight at 4°C to label actin, followed by an additional three 15 min washes in 0.02% Tween. Finally, samples were counter-stained with DAPI (1:500 dilutions; Sigma-Aldrich, D9542) to visualize nuclei.

Calculation of Elongation Angles

Images were taken using a Zeiss Z1 inverted microscope, 20x objective. Cantilevers were normalized to 0°. Images were acquired, inverted, applied a threshold and made binary. The Particle Analyzer plugin was employed to fit an ellipse to each cell. The angle of the major axis was reported.

Calculation of Outgrowth Distance

Outgrowth distances of spheroids were calculated by linear distance of furthest cell tip from the center of the spheroid in the direction of alignment, divided by the linear distance of the furthest cell tip in the direction of tension.

Mechanical Testing

Harvested mammary tumors were tested in compression on a uniaxial Enduratec ELF3200 load frame (Bose Electroforce, Eden Prairie, MN) to 30% and 50% strain at a rate of 2%/s. Resulting stress and strain were calculated from the resulting load-displacement data.

Collagen gels at 2mm thickness were prepared and irradiated at the doses described using a Mark I Model 68 Cesium Gamma Irradiator operated under NIH Grant: S10RR023781. Tensile dog bone punches were taken from each sample with a gauge length of 5mm. Each tensile sample was tested to failure at a strain rate of 3%. Resulting load data was analyzed for the tensile modulus by least square regression over the elastic region of the curve. Compressive samples were taken from irradiated collagen gels using a 6mm circular biopsy punch. Each sample was tested under confined stress relaxation compression to 30% strain in increments of 5%. Using a custom MATLAB program (Mathworks, Natick, MA) a poroelastic model was fit to the data and analyzed for gel equilibrium and instantaneous stiffness, as well as hydraulic permeability (149).

Permeability Assay

Collagen gels were transferred into ThinCert™ polyethylene terephthalate (PET) membrane 6-well cell culture inserts with 0.8μm pore size (Greiner Bio-One) and incubated for 45min at 37°C for polymerization. Treatment gels were then given a

dose of 63Gy. For the assay, 1mL of 10μM 40kDa FITC-dextran (Sigma, St. Louis, MO, USA) in complete media was added to the upper chamber, while 2mL of complete media was added to the lower chamber. 100μL samples were collected from the lower compartment and placed into a glass bottom 96 well-plate, then replaced with equal volume of complete media every 20min for 4hrs. A 200μm z-slice of each sample was captured using a Zeiss LSM700 confocal microscope on a Zeiss Axio Observer Z1 inverted stand equipped with a long-working-distance water-immersion 40X/1.1 numerical aperture Zeiss objective at 488nm. Fluorescent intensity was then measured in ImageJ (v2.0.0-rc-41/1.50d, National Institutes of Health, Bethesda, MD, USA) from a 150x75μm "Region of Interest" (ROI) approximately 10μm from the bottom of each well.

IR Spectroscopy of Irradiated Collagen Scaffolds

1mg/mL collagen samples were analyzed using Fourier Transform Infrared (FT-IR) spectra obtained from a Thermo Scientific Nicolet iS10 (161, 162). Backgrounds were acquired from the media used to make the collagen as described earlier under Collagen Preparation. Scans were obtained at a resolution of $4cm^{-1}$ between $700\text{-}2000cm^{-1}$.

Mice

All mice were maintained following a protocol approved by the Cornell University Institutional Animal Care and Use Committee. MMTV-PyMT transgenic mice from the FVB strain background were obtained from the Jackson Laboratory. Mammary

tumors were excised from 10-12 week old female MMTV-PyMT transgenic mice. The freshly isolated mammary tumors were immediately irradiated and then flash frozen in liquid nitrogen before mechanical testing and later thawed as described previously (163).

Cell Adhesion and Spreading

Cell adhesion and spreading studies were performed on 2.5 mg/mL collagen. 100 cells/cm^2 were seeded on top of untreated or irradiated collagen gels. After being allowed to attach and spread for the indicated time, cells were washed 3 times with 1X PBS and fixed with 3.7% formaldehyde in PBS for 15 min. Cells were stained for DAPI or phalloidin-Alexa Fluor® 564 and imaged through 35 mm plastic petri dishes. Acquired images were analyzed in ImageJ.

Cell Invasion

Cell invasion studies were performed in a 6-well plate with transwell insert containing 8μm pores. A 500 μm layer of collagen was polymerized on top of the transwell membrane. 5,000 cells/cm^2 were seeded on top of the collagen. 1ml of serum-poor media (DMEM with 5% FBS and 1% Pen Strep) was placed in the transwell. Outside the transwell, contained by the well plate, 2mL of serum-rich media (DMEM with 10% FBS 1% Pen Strep) is placed. Serum gradient was replaced every 48hrs for 7 days. After 7 days, the bottom of the transwell is treated with 0.25% Trypsin and rinsed twice with 1X PBS to remove adherent cells. The wellplate is then fixed with

3.7% formaldehyde PBS for 15min and stained with DAPI. Fluorescent images are taken and quantified with ImageJ particle analyzer. The transwell is placed in a new 6 well plate and the serum gradient is reestablished. The process is repeated every 24hrs for two additional days.

PVDF Preparation

To prepare the PVDF for electrospinning, 15%wt is dissolved into a solvent mixture of acetone and DMF in a ratio of 30/70, respectively. In common practice[14], the PVDF is first dissolved in the DMF, stirred for 24 hours, after which the acetone is added and stirred for another 24 hours at room temperature.

Electrospun Collagen Preparation

The procedure follows the common practice of lyophilized collagen being dissolved in .083g/ml 1,1,1,3,3,3 hexafluoro-2-propanol (HFP)[15]. Once the collagen is full dissolved it is taken up by a syringe and mounted to a syringe pump.

Electrospinning Process

With a conventional electrospinning system, the viscous PVDF solution is loaded into a syringe (needle diameter = 0.45mm), placed horizontally into a programmable syringe pump and extruded at a rate of 3ul/m. Similarly, the collagen solution is mounted to a second syringe pump and extruded at 3ul/m. Both syringes feed into a custom coaxial needle with the PVDF attached to the inner bore. The voltage applied to the needle was set to 15kV and placed 12cm above the ground electrode.

The electrospinning process creates a characteristic "whipping" motion resulting in randomly oriented fibers. However, bias voltages in the fiber trajectory can influence deposition position. The goal is to be able to sweep the fiber trajectory over the glass slide. A device built to achieve this is described in the next subsection.

Modulating Fiber Stiffness

By increasing the field strength between the two ITO plates, suspended fibers will contract proportional to the d_{31} piezoelectric coefficient of PVDF[16]. This will have the effect of creating slack in the fiber. Reversing the field will cause "negative contraction" (expansion) and the fiber will experience an increase in stiffness.

Taking Sim-Pol Images

Structurally illuminating polarized light followed the following procedure: Place the Rochi Ruling in the top slide holder located between the condenser and the light source. Peering through the eyepieces, adjust the condenser until the ruling is in clear focus. Remove any optics between the ruling and the eyepieces (except for the condenser), place your sample in the motorized sample holder (Moves in z-direction). Adjust the objective/sample/condenser until both the ruling and a plane of the sample are in clear focus. Set the ADP Thor Labs software to move the micrometer controlling the Rochi ruling 2pi/3 (this distance is dependent upon the lines/mm of your ruling). Place the micrometer that holds the polarizer in between the Rochi ruling and the top of the condenser. Set the ADP Thor Labs software controlling the polarizer

to move through 180 degrees in a minimum of 4 steps. (More steps helps reduce some noise). Check to make sure the ruling and the sample are in focus and place the circular polarizer at 0 degrees after the objective (10xP or 20xP). Use the micrometer control to adjust the polarizer until total extinction occurs (darkest possible setting) and take this picture. Use the ADP software to move the rochi ruling 2pi/3. Take this picture. Repeat the last two previous steps. Use the ADP software to rotate the polarizer you 180/x turns degrees. Take this picture. Move the rochi ruling 2pi/3. Take this picture and repeat for each polarizer angle until 180 degrees have been accounted for. Organize all these images into sets of 3 ruling images for every 1 polarizer setting. Use the ADP Software to move the sample into a new plane (~1-20um depending on desired z-resolution). Repeat the entire process starting for each new z-plane in the sample. Execute MATLAB code to reconstruct each of the sets (SIM Reconstruction). Execute MATLAB code to reconstruct Polarized Light Microscopy Images (qPOL Analysis). Execute MATLAB 3D Imaging of this final stack to see 3D Super-Resolution, Stress/Strain/Alignment image.

Irradiating MDA-231 For Invasion Studies

In order to prep the collagen for irradiation pre-seeding, the following protocol was followed: Prepare collagen at desired density (typically 1-3mg/ml). Spread 200ul to 500ul across each transwell, first lining the rim and then making an "X" through the middle. "Paint" the transwell with the pipette being very careful not to puncture the mesh. Incubate for 30min or until collagen is polymerized. Irradiate wells using the following metric: 1min = 5Gy. Add a known cell density to each well (1ml at

~100k/ml). Add 2ml of Complete DMEM to bottom of the well. Add 1ml of Serum Starved Media to transwell with cells and allow to incubate for 3-7 Days, or until cells begin to transverse the collagen. Stain/Image cells at the bottom of the well and count.

Building Single Fiber 1-D Matrices

To produce activated, electrospun pvdf collagen fibers the following procedure was followed: Spin coat PDMS solution onto ITO Glass Slides and cut out cured PDMS planks/bars to line the sides of the glass leaving a small 1-2mm gap between them. Place the assembly off-center of the electrospinning needles direct path and at a slight angle (~10-15 degrees) by putting a folded piece of paper or something non conductive under one of the edges. Place the needle tip ~20mm from Ground Plane. Set the syringe pump to 0.1 ml/hr. Set the HV to 12.8-13.0 kV. Observe through camera when a single fiber whips out across the assembly gap. Happens about 1-2 times a minute. (Occurs more frequently at first and less so later as humidity and solvent % vapor increases in the chamber). PVDF dissolves nicely in 50/50 DMF/THF at 8% m/V but playing with this makes the fibers thicker, stronger, etc.